Meteoritics & Planetary Science 40, Nr 12, 1789–1812 (2005)
Abstract available online at http://meteoritics.org

Impactites of the Haughton impact structure, Devon Island, Canadian High Arctic

Gordon R. OSINSKI[1†*], John G. SPRAY[1], and Pascal LEE[2]

[1]Planetary and Space Science Centre, Department of Geology, University of New Brunswick,
2 Bailey Drive, Fredericton, New Brunswick E3B 5A3, Canada
[2]Mars Institute, SETI Institute, and NASA Ames Research Center, Moffett Field, California 94035–1000, USA
[†]Canadian Space Agency, 6767 Route de l'Aeroport, Saint-Hubert, Quebec, J3Y 8Y9, Canada
[*]Corresponding author. E-mail: osinski@lycos.com

(Received 07 April 2004; revision accepted 08 November 2004)

Abstract–Contrary to the previous interpretation of a single allochthonous impactite lithology, combined field, optical, and analytical scanning electron microscopy (SEM) studies have revealed the presence of a series of impactites at the Haughton impact structure. In the crater interior, there is a consistent upward sequence from parautochthonous target rocks overlain by parautochthonous lithic (monomict) breccias, through allochthonous lithic (polymict) breccia, into pale grey allochthonous impact melt breccias. The groundmass of the pale grey impact melt breccias consists of microcrystalline calcite, silicate impact melt glass, and anhydrite. Analytical data and microtextures indicate that these phases represent a series of impact-generated melts that were molten at the time of, and following, deposition. Impact melt glass clasts are present in approximately half of the samples studied. Consideration of the groundmass phases and impact glass clasts reveal that impactites of the crater interior contain shock-melted sedimentary material from depths of >920 to <1880 m in the pre-impact target sequence.

Two principal impactites have been recognized in the near-surface crater rim region of Haughton. Pale yellow-brown allochthonous impact melt breccias and megablocks are overlain by pale grey allochthonous impact melt breccias. The former are derived from depths of >200 to <760 m and are interpreted as remnants of the continuous ejecta blanket. The pale grey impact melt breccias, although similar to the impact melt breccias of the crater interior, are more carbonate-rich and do not appear to have incorporated clasts from the crystalline basement. Thus, the spatial distribution of the crater-fill impactites at Haughton, the stratigraphic succession from target rocks to allochthonous impactites, the recognition of large volumes of impact melt breccias, and their probable original volume are all analogous to characteristics of coherent impact melt layers in comparatively sized structures formed in crystalline targets.

INTRODUCTION

A wide variety of impactites ("rock affected by impact metamorphism") (Stöffler and Grieve 1994, 1996) are produced during hypervelocity impact events, although they can be classified into three major groups: (1) shocked rocks; (2) impact breccias; and (3) impact melt rocks.[1] The presence, distribution, and characteristics of impact melt rocks have provided valuable information on the cratering process (e.g., Dence 1971; Grieve et al. 1977; Grieve and Cintala 1992). Coherent impact melt rocks often display classic igneous features (e.g., columnar jointing) and textures (e.g., glassy or fine-grained crystalline groundmass), and are easily recognizable as products of crystallization from a melt (see Dressler and Reimold 2001 for a review). It is widely accepted that coherent impact melt rocks only form in impact structures developed in predominantly crystalline (e.g., the Manicouagan, Mistastin, and West Clearwater Lake impact structures, Canada) or mixed crystalline-sedimentary targets (e.g., Popigai, Russia). In the latter case, the impact melt rocks and glasses are apparently derived entirely from the crystalline basement (e.g., Masaitis 1994; Whitehead et al. 2002).

In impact structures formed in predominantly sedimentary (and principally carbonate-rich) target rocks,

[1]Note that impact melt rocks are further subdivided into clast-free, clast-poor, or clast-rich (i.e., impact melt breccias), depending on their clast content. Impact breccias do not contain melt in the matrix/groundmass, but can contain clasts of impact melt glass.

impact melt rocks have not generally been recognized. The resultant impactites have been referred to as lithic, clastic matrix, or fragmental breccias that are supposedly melt-free (e.g., Kieffer and Simonds 1980; Redeker and Stöffler 1988; Stöffler and Grieve 1996). When recognized, it has been widely documented that the volume of impact melt rocks found in impact structures developed in sedimentary targets is about two orders of magnitude less than for crystalline targets in comparably sized impact sites (Kieffer and Simonds 1980). This anomaly has been attributed to the generation and/or release of enormous quantities of sediment-derived volatiles (e.g., H_2O, CO_2, SO_x), resulting in the wide dispersion of shock-melted sedimentary rocks (Kieffer and Simonds 1980).

However, Osinski and Spray (2001, 2003) have recently presented evidence from the Haughton impact structure that is in disagreement with previous models of the response of sedimentary rocks, in particular carbonates, to hypervelocity impact. Combined field, optical, and analytical scanning electron microscope (SEM) studies reveal that calcite, silicate glass, and anhydrite in the groundmass of pale grey impactites of the crater interior at Haughton represent a series of impact-generated melts that were molten at the time of, and following, deposition (Osinski and Spray 2001, 2003). These impactites can, therefore, be termed impact melt breccias or clast-rich impact melt rocks (Osinski and Spray 2001, 2003), according to the terminology of Stöffler and Grieve (1994, 1996). Carbonate melt-rich impactites have also been documented at the Ries (Graup 1999; Osinski 2003; Osinski et al. 2004) and Chicxulub (Jones et al. 2000; Claeys et al. 2003; Dressler et al. 2004; Kring et al. 2004; Stöffler et al. 2004; Tuchscherer et al. 2004) impact structures.

Here we present the results of detailed mapping of the Haughton structure, which reveal the presence of a series of additional impactite types, including previously unrecognized ejecta deposits and other impactites in the crater interior (see map insert). These provide insight into the processes and products of hypervelocity impact into sedimentary targets. A complete petrographic study of all impactites at Haughton (i.e., shocked rocks, impact breccias, and impact melt rocks/breccias) is outside the scope of this contribution. Thus, in this work we have focused on the petrography of the major (in terms of volume) impact melt-bearing allochthonous impactites. In particular, we have extended earlier investigations of the groundmass of the pale grey impactites of the crater interior at Haughton. New data on the modal abundance and composition of groundmass phases are presented here, along with an investigation of glass clasts and modal abundances of lithic and mineral clasts. Petrographic studies of impactites from the crater rim region have been carried out for the first time.

GEOLOGICAL SETTING OF THE HAUGHTON IMPACT STRUCTURE

Haughton is a well-preserved complex impact structure 23 km in diameter that is situated on Devon Island in the Canadian Arctic Archipelago (75°22′N, 89°41′W) (Fig. 1). Recent ^{40}Ar-^{39}Ar dating of potassic glasses yields an age of 39 ± 2 Ma (Sherlock et al. 2005) for the Haughton impact event, making this crater substantially older than previously thought (23.4 ± 1.0 Ma) (Jessburger 1988). The pre-impact target sequence at Haughton comprised a ~1880 m thick series of Lower Paleozoic sedimentary rocks of the Arctic Platform, overlying Precambrian metamorphic basement rocks of the Canadian Shield (Fig. 1c) (Frisch and Thorsteinsson 1978; Osinski et al. 2005). This value of 1880 m represents the thickness to the top of the Upper Member of the Allen Bay Formation, which was the youngest sedimentary unit present in the Haughton region at the time of impact (Frisch and Thorsteinsson 1978; Thorsteinsson and Mayr 1987; Osinski et al. 2005). The unmetamorphosed sedimentary succession consists of thick units of dolomite and limestone, with subordinate evaporite horizons and minor shales and sandstones (Fig. 1c) (Thorsteinsson and Mayr 1987). Carbonates and evaporites comprise ~75–80% and ~8%, respectively, of the target sequence at Haughton (Fig. 1c) (Osinski et al. 2005). This stratigraphically conformable sequence of early Cambrian to Siluro-Devonian rocks lies in a gently west-dipping homoclinal succession, which exposes approximately north-south striking layers that young to the west. Post-impact lacustrine sediments of the Haughton Formation (Hickey et al. 1988) unconformably overlie both the crater-fill impactites and pre-impact target rocks (Frisch and Thorsteinsson 1978; Osinski and Lee 2005). Importantly, it has recently been shown that the Haughton Formation post-dates the Haughton impact event by several Ma (Osinski and Lee 2005; Sherlock et al. 2005).

SAMPLES AND ANALYTICAL TECHNIQUES

Field studies, including detailed 1:25,000 scale mapping, were conducted over the course of five field seasons (see map insert). More than 350 samples of impactites were collected from the crater-fill deposits at Haughton. They consist of hand specimens of impact breccias and impact melt breccias and individual clasts from within these lithologies. Polished thin sections were prepared from 90 of these samples and these were investigated using a JEOL 6400 digital scanning electron microscope (SEM) equipped with a Link Analytical eXL energy dispersive spectrometer (EDS) and Si(Li) LZ-4 Pentafet detector. Mobilization of alkalis was reduced by using raster scan modes and varying count times from 60 to 100 sec. Beam operating conditions were 15 kV and 2.5 nA at a working distance of 37 mm. The beam diameter was ~1 µm, with a beam penetration of ~2–4 µm, depending on the phase being analyzed. Analyses were calibrated using a multi-element standards block (Type 202-52) produced by the C.M. Taylor Corporation of Sunnyvale, California. SEM backscattered electron (BSE) imagery was used to investigate the microtextures of the impact glasses, accompanied by

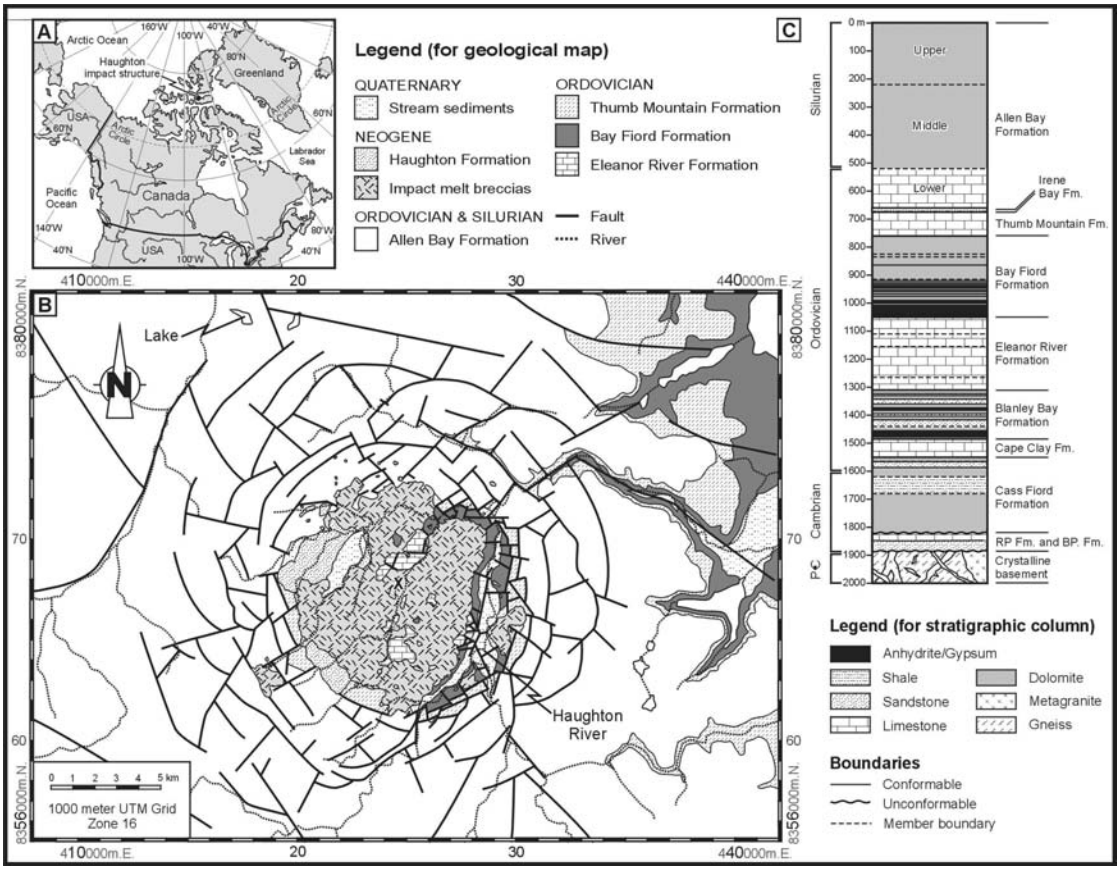

Fig. 1. a) Location of the Haughton impact structure in the Canadian High Arctic. b) Simplified geological map of the Haughton impact structure. "X" = location of Anomaly Hill. See the map insert in this issue for an enlarged and more detailed map of Haughton. c) Stratigraphic column showing the target sequence at the Haughton impact structure. Abbreviations: Fm. = Formation; RP = Rabbit Point; BP = Bear Point. Compiled with data from Thorsteinsson and Mayr (1987) and two of the author's field observations (G.R.O. and P.L.).

single spot analysis of individual particles. X-ray diffraction (XRD) was performed on powdered samples using a Philips 1710 diffractometer and generator, with operating conditions of 40 kV and 20 mA. The clast content and modal composition of the samples studied were measured on representative digital BSE images using an image analysis program (Scion Image).

FIELD RELATIONS

Haughton is easily recognizable from the air due to the distinctive light grey impactites in the center of the structure that contrast with the surrounding monotonous brown-colored sedimentary rocks of the Arctic Platform (see Landsat-7 satellite image on front cover of this issue). These impactites constitute the bulk of the allochthonous crater-fill at Haughton and they currently form a discontinuous 53.8 km^2 layer in the central area of the structure (Fig. 1; map insert). Seismic reflection data (Scott and Hajnal 1988) and field studies reveal that the crater-fill has a maximum current thickness of ~125 m, with a present volume of ~7 km^3. The presence of pale grey crater-fill impactites up to ~140 m above the central topographic low area suggests that the original thickness exceeded 200 m. Isolated outcrops over an area up to ~12 km in diameter further suggest that the crater-fill originally completely occupied the central area of the crater. This view is supported by the results of shallow drilling and recent field studies that reveal the presence of pale grey impactites underlying the main expanse of the Haughton Formation sediments (Osinski and Lee 2005). Assuming an approximately circular deposit (~12 km diameter) and a conservative estimate of ~200 m for its average thickness, the original volume of the crater-fill is estimated to be >22.5 km^3.

Previous workers have considered the grey crater-fill impactites at Haughton as a single impactite lithology ("polymict impact breccia") (Metzler et al. 1988; Redeker and Stöffler 1988). However, detailed mapping as part of this study reveals that several different types of impactites are present at Haughton (Fig. 2; map insert). A distinction is made here between impactites in the interior of the crater (radial range from crater center <6 km; i.e., crater-fill lithologies within the collapsed transient cavity), and those of the near-surface crater rim region (i.e., lithologies that have been transported from their place of origin in the original transient cavity).

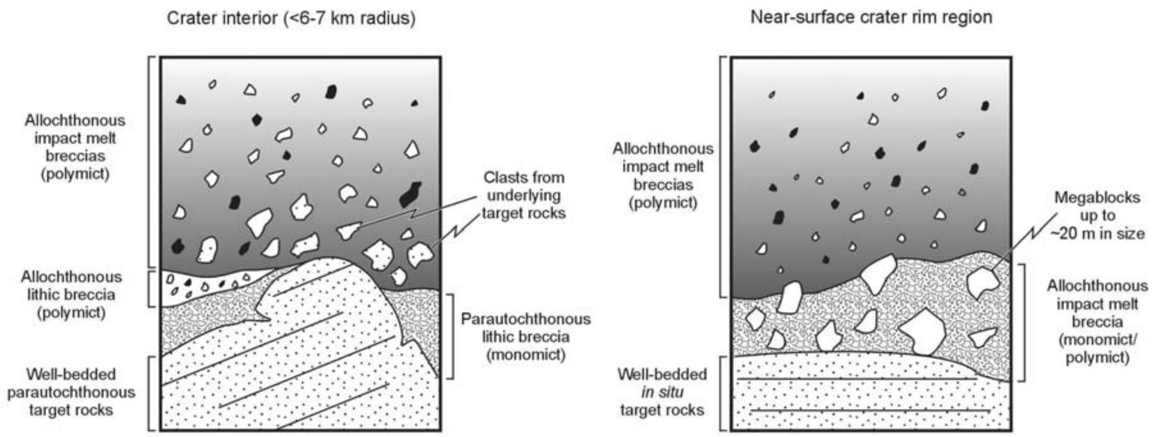

Fig. 2. Schematic cross-sections showing the different types of impactites and their stratigraphic sequence in the crater interior (a) and near-surface crater rim (b) regions of the Haughton impact structure.

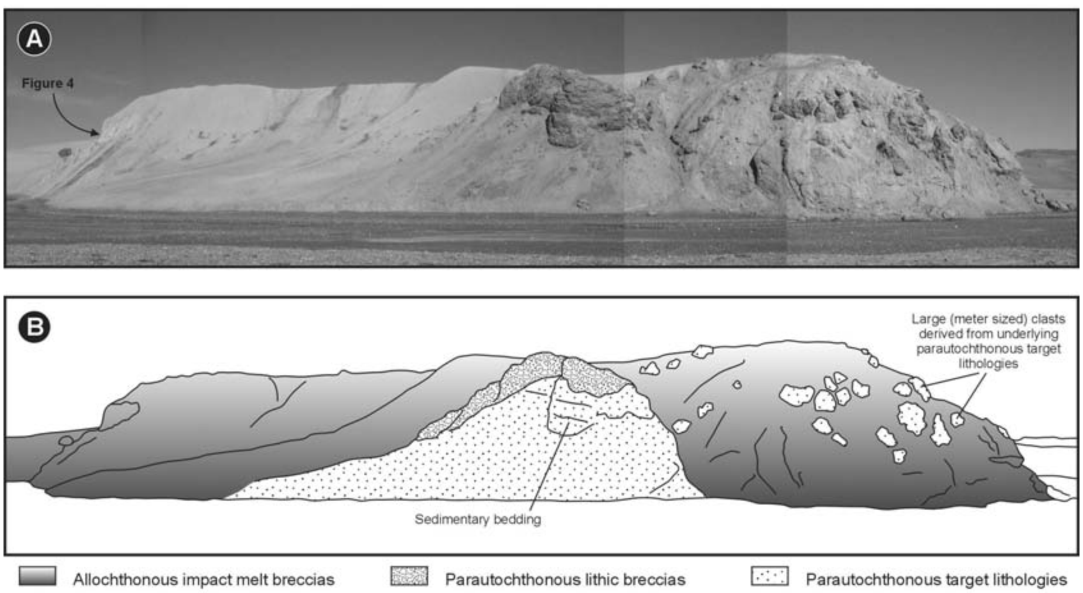

Fig. 3. Panoramic field photograph (a) and line drawing (b) showing the transition from parautochthonous target rocks of the central uplift (Bay Fiord Formation evaporites and limestones in this image), into pale grey crater-fill impact melt breccias. Large clasts (up to ~5 m in diameter) of the underlying uplifted target material are present in the base of the impact melt breccia layer. Point of view of Fig. 4 is shown in (a).

Crater Interior

The pale grey crater-fill impact melt breccias are typically heavily weathered, mainly due to periglacial processes (e.g., solifluction and gelifluction), with only sparse outcrops. The best exposures occur in the north and east of the structure along incised river valleys (Fig. 1b; map insert). The field relations between the crater-fill impact melt breccias and the underlying target rocks have been studied in detail at a series of outcrops along the Haughton River and Rhinoceros Creek valleys (map insert). There is a consistent upward sequence of lithologies from target rocks to impact melt breccias (Fig. 2a):

1. Shallow to steeply dipping (~10–80°) parautochthonous target rocks with an increase in the intensity of fracturing upwards (Fig. 3). Aside from this fracturing, the only obvious sign of deformation is the tilted nature of the bedding and the occasional presence of shatter cones in carbonate lithologies.
2. Parautochthonous lithic breccia (monomict) up to a maximum current thickness of ~10 m, derived from underlying target rocks (Fig. 3). These breccias are clast-supported, with typical clast contents of ~60–80 vol%. This unit varies significantly in appearance across the crater due to derivation from different local target lithologies (e.g., predominantly evaporites in the east

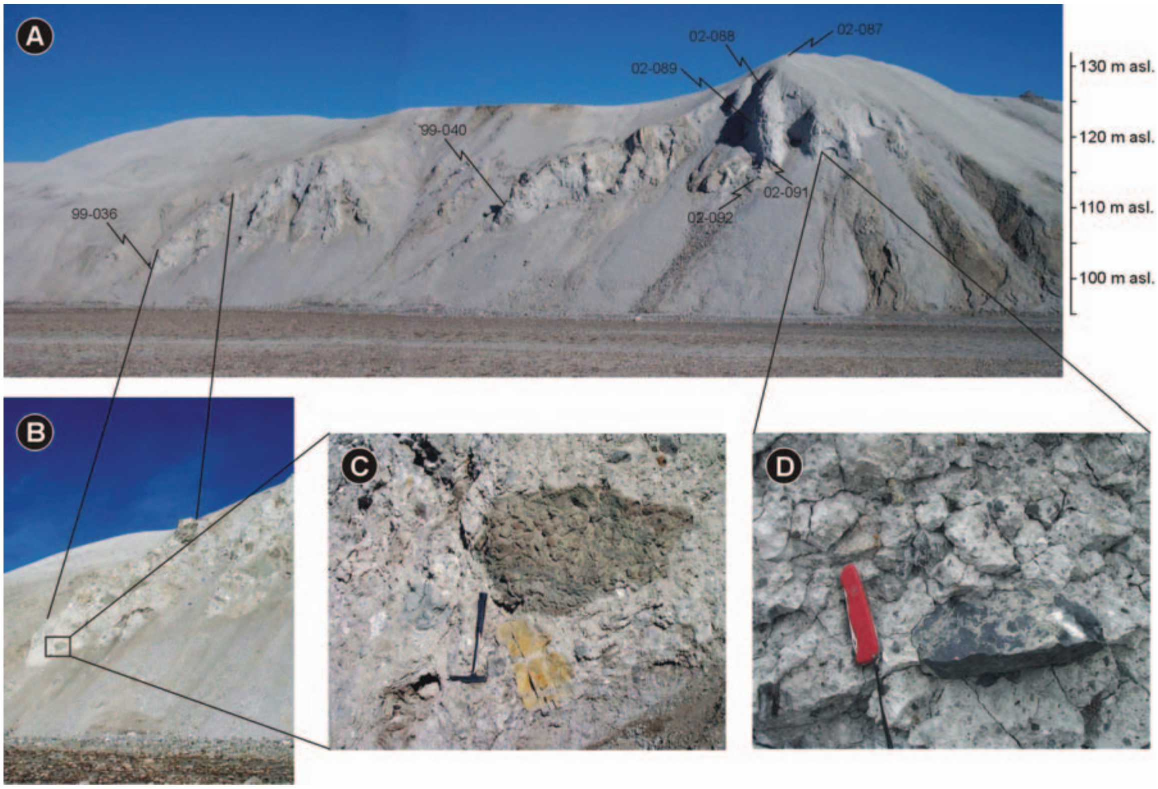

Fig. 4. a) A panoramic field photograph of a well-exposed cross-section through the base of the crater-fill impact melt breccias; sample locations are shown. Note that the average clast size decreases upwards. b) and c) Close-up views of the lower levels of the crater-fill impact melt breccias, which are typically clast-rich with above average (i.e., meter length) clast sizes. At this locality, large clasts from the lower levels of the sedimentary sequence (e.g., shale) and the crystalline basement (e.g., gneiss) can be seen. A 40 cm long rock hammer is shown for scale in (c). d) A close-up view of impact melt breccias at a higher level than previous views (b and c). The majority of clasts in this picture are carbonates. At this height in the outcrop, clasts rarely exceed ~20–30 cm in diameter. Also note the fine-grained microscopic nature of the pale grey groundmass. A 12 cm long penknife is shown for scale. The highest point at the right of the picture is located at 426,050 m.E. 8,371,266 m.N.

and carbonates in the west). The contact with the underlying target rocks is typically gradational and occurs over short distances of <50 cm.

3. Friable, allochthonous, lithic breccia (polymict) with clasts derived from a wide range of target lithologies, set in a fine-grained clastic matrix, which forms up to ~30 vol% of the unit (i.e., these breccias are typically clast-supported). No clasts from the crystalline basement are present. Clasts of limestone and dolomite commonly display well-developed shatter cones. This unit appears to be discontinuous and ranges in thickness up to ~4 m.
4. Allochthonous impact melt breccias with a sharp and typically irregular contact with the underlying allochthonous and/or parautochthonous lithic breccias. The lower levels of the impact melt breccias are clast-rich, with above average (i.e., meter length) clast sizes (Figs. 3 and 4). This has been termed a "basal megabreccia" by Osinski and Spray (2003). The megabreccia in Fig. 3 contains abundant, large (up to ~5 m in diameter) unshocked/lightly shocked (~1–2 GPa) blocks of Bay Fiord Formation evaporites, derived from underlying parautochthonous target rocks. The impact melt breccias comprise a microscopic groundmass containing variably shocked lithic and mineral clasts from a wide range of target lithologies, including clasts from the crystalline basement (Figs. 4c and 4d) (Metzler et al. 1988). The fine-grained groundmass is locally intrusive, with irregular veins penetrating up to ~80 cm into some of the larger lithic clasts. The main mass of the pale grey crater-fill impactites (i.e., ~10–20 m above the base) is characterized by slightly better sorting, with the majority of clasts having dimensions <25 cm (Fig. 4). There are no indications of layering or preferred orientation of clasts.

Near-Surface Crater Rim Region

Detailed mapping has revealed the existence of a series of impactites in the near-surface crater rim area of Haughton (Fig. 2b; map insert). Two principal impactites have been recognized (from the base upwards) (Fig. 2b):

Fig. 5. A field photograph of allochthonous yellow-brown impact melt breccias from the crater rim region, which contain large megablocks. These impactites are polymict at the hand specimen scale; however, at this locality (418,920 m.E. 8,364,550 m.N.), all clasts are derived from the Thumb Mountain Formation (see Fig. 1c). The primary author (G.R.O.) is in the foreground for scale. The inset shows a hand specimen photograph of the impact melt breccia from this locality.

1. Yellow-brown allochthonous impact breccias with a microscopic, pale yellow groundmass (Fig. 5). These impactites are polymict, in as much as different clast types are present; however, at a given locality, all clasts are derived from the same formation. The target lithologies present in these breccias range from the Middle Member of the Allen Bay Formation (>200 to <500 m pre-impact depth) to the Thumb Mountain Formation (>680 to <760 m pre-impact depth). There is a large range in clast size from a few millimeters to >10 m in size (Fig. 5). The latter have been termed megablocks in keeping with studies at other terrestrial impact sites (e.g., the Ries impact structure, Germany; Pohl et al. 1977). Many of the megablocks contain well-developed shatter cones and fossil horizons indicating an overturned stratigraphy. The exterior surfaces of the megablocks are commonly highly polished, with well-developed lineations that resemble slickenside fault lineations.
2. Pale grey impact breccias, the largest occurrence of which is preserved in a down-faulted graben in the southwest of the Haughton structure (Fig. 1; map insert). These impactites resemble the crater-fill impact melt breccias; however, there are important differences in composition and modal abundance of groundmass phases and clasts (see below). Also, the pale grey crater rim impactites have a smaller average clast size and lack the basal megabreccia seen in the crater interior. The preservation of these impactites in down-faulted grabens suggests that they were originally more widely distributed.

PETROGRAPHY OF CRATER-FILL IMPACT MELT BRECCIAS

Impact melt breccias in the interior of the Haughton structure comprise a microscopic groundmass containing variably shocked mineral and lithic clasts from a wide range of target lithologies (Frisch and Thorsteinsson 1978; Metzler et al. 1988; Redeker and Stöffler 1988; Osinski and Spray 2001, 2003). The modal abundance in thin section of groundmass and clast types of representative samples from these impactites is given in Table 1. It is notable that the crater-fill impact melt breccias are clast-rich, typically containing ~40–50 vol% clasts, although some exceptions do occur (e.g., ~10–30 vol% clasts in samples 99-045a and 00-220) (Table 1). Details are given below on the characteristics of the groundmass and clasts, in respective sections. (Note that we define the groundmass as the fine-grained material that encloses fragments of shocked and unshocked target material.)

Groundmass

Two main points are of note: (1) crater-fill impact melt breccias are typically groundmass-supported; and (2) the proportion of the various groundmass phases and clasts varies considerably, both between different localities and outcrops

Table 1. Modal composition of crater-fill impact melt breccias (all data in vol%)[a].

	UTM position		Groundmass				Clasts						
Sample #	Easting	Northing	Cal	Gls	An	Tot	Dol	Lst	Evp	Sst	Xst	Gls	Tot
99-001	428,350	8,368,860	12.8	36.4	–	49.2	37.5	–	–	1.5	11.8	–	50.8
99-007	428,320	8,368,870	10.2	10.0	29.2	49.4	30.8	3.5	9.4	0.6	2.6	3.7	50.6
99-009	427,320	8,371,060	22.8	29.6	–	52.4	36.2	6.1	1.5	1.0	2.8	–	47.6
99-015	427,134	8,368,960	14.7	40.4	–	55.1	37.2	–	6.4	0.6	0.7	–	44.9
99-021	428,300	8,369,090	25.1	32.2	–	57.3	34.3	5.5	–	0.9	1.3	0.7	42.7
99-044	426,230	8,371,190	11.5	10.9	36.3	58.7	21.1	1.9	8.3	0.6	–	10.4	42.3
99-045[a]	426,320	8,371,190	9.8	0.3	60.5	70.6	20.0	0.5	7.6	0.5	0.8	–	29.4
99-065	424,930	8,368,240	16.4	31.8	–	48.2	33.0	–	–	3.6	3.6	11.6	51.8
99-105[b]	429,230	8,369,760	56.3	–	–	56.3	39.4	1.2	–	–	3.1	–	43.7
00-023	420,560	8,370,930	18.0	33.5	–	51.5	41.0	1.1	–	0.4	4.7	1.3	48.5
00-046	422,150	8,372,800	18.8	37.9	–	56.7	32.9	0.9	–	0.3	7.6	1.6	43.3
00-220	425,340	8,372,410	52.1	35.8	–	87.9	11.4	0.5	–	0.1	0.1	–	12.1
00-257	427,920	8,368,440	6.7	41.0	–	47.7	38.8	1.7	–	0.5	3.2	8.1	52.3
00-288	426,120	8,370,680	37.8	19.3	–	57.1	37.5	1.8	–	1.3	–	2.3	42.9
02-003	419,860	8,366,460	20.6	33.8	–	54.4	41.8	3.7	–	0.1	–	–	45.6
02-012	418,000	8,364,080	26.9	32.6	–	59.5	37.9	2.6	–	–	–	–	40.5
02-074	423,350	8,371,180	19.0	34.6	–	53.6	45.6	0.8	–	–	–	–	46.4
02-087	426,050	8,371,250	19.5	28.9	–	48.4	41.3	3.2	–	1.1	0.4	5.6	51.6
02-088	426,030	8,371,240	23.1	31.7	–	54.8	43.1	0.1	–	0.3	0.2	1.5	45.2
02-090	426,030	8,371,230	26.7	26.6	–	53.3	39.9	0.2	–	0.2	1.1	5.3	46.7
02-092	426,030	8,371,220	28.8	26.4	–	55.2	39.0	0.8	–	0.4	0.9	3.7	44.8
02-119	423,680	8,372,930	19.7	34.1	–	53.8	35.4	1.0	–	0.5	3.3	6.0	46.2
02-133	422,400	8,370,580	27.0	32.6	–	59.6	36.1	3.1	–	0.7	0.3	0.2	40.4

[a]Abbreviations: Cal = calcite; Gls = silicate impact melt glass; An = anhydrite; Tot = total; Dol = dolomite; Lst = limestone; Evp = evaporite (gypsum and/or anhydrite); Sst = sandstone; Xst = crystalline.
[b]All groundmass phases in sample 99-105 have been hydrothermally altered and replaced by calcite, celestite, and minor fluorite.

(Table 1), and over the scale of a thin section (Fig. 6). Dolomite was previously thought to be the predominant groundmass/matrix forming phase (Redeker and Stöffler 1988); however, SEM studies reveal that the groundmass of these impactites consists of three main components (Table 1): (1) microcrystalline calcite; (2) silicate impact melt glass; and (3) anhydrite. The analytical SEM, with its greater resolution, reveals that dolomite always occurs as shocked angular fragments within the groundmass (e.g., Fig. 6), and should not, therefore, be considered a true groundmass-forming phase (cf. Osinski and Spray 2001). The various groundmass phases typically comprise ~50–60 vol% of the crater-fill impact melt breccias (Table 1). A detailed description of the three main groundmass components follows.

Calcite

Calcite is present as a groundmass-forming phase in all of the samples studied, comprising, on average, ~20–25 vol% of the crater-fill impact melt breccias (Table 1), although there is a considerable range (<10 to >50 vol%) (Table 1). There is a continuous transition from samples rich in calcite (Figs. 6a and 6b), through samples consisting of finely dispersed calcite in silicate glass (Figs. 6c–e), to regions of samples consisting predominantly of silicate glass, with only irregularly shaped blebs of calcite (Fig. 6f). Our observations and data confirm the findings of Osinski and Spray (2001) that groundmass-forming calcite is a primary impact melt phase. Evidence for this includes: (1) intermingling, but not blending, of calcite with silicate glass (e.g., Figs. 6c and 6d); (2) individual spheres of calcite within the groundmass (e.g., Fig. 6c); (3) rounded calcite grains in silicate glass (e.g., Figs. 6c–f), which is typical for calcite that has crystallized from a melt (e.g., Lee and Wyllie 2000); (4) curved menisci with sharp boundaries between silicate glass and calcite (e.g., Figs. 6c and 6d); (5) evidence for the assimilation of dolomite clasts, which required temperatures in excess of ~1050 K (Otsuka 1986); (6) flow textures and injections of calcite into clasts, indicating that the calcite phase was originally a fluid; and (7) overgrowths (often euhedral) of calcite on dolomite clasts (e.g., Fig. 6e), similar to phenocryst/xenocryst-groundmass relationships that are common in silicate igneous rocks.

EDS analyses of groundmass-forming calcite are presented in Table 2 and illustrated in Fig. 7. In general, groundmass-forming calcite of the crater-fill impact melt breccias have relatively higher MgO (up to ~2.0 wt%), FeO (up to ~0.5 wt%), and SiO_2 (up to ~7.3 wt%) than calcite phases analyzed in sedimentary target material and post-impact hydrothermal products (Tables 2, 3). The former are also rich in Al_2O_3, K_2O, and SO_3, compared to the latter (Tables 2 and 3). These observations are in agreement with

Table 2. Average composition of groundmass-forming calcite in crater-fill impactites[a].

Sample #	99-007		99-015		99-044		99-045xb		99-065		00-220	
Number of analyses	6		3		4		5		4		3	
	wt%	s.d.	wt%	s.d.	wt%	s.d.	wt%	s.d.	wt%	s.d.	wt%	s.d.
SiO_2	2.49	3.18	3.08	3.25	7.35	6.45	0.84	2.27	0.45	0.46	–	n.d.
Al_2O_3	0.48	1.46	0.52	0.93	2.20	1.47	0.39	1.50	0.17	0.46	–	n.d.
FeO	0.03	0.16	0.07	0.24	0.45	0.18	0.42	1.68	0.10	0.23	–	n.d.
MnO	–	n.d.	–	n.d.	0.07	0.32	–	n.d.	–	n.d.	–	n.d.
MgO	1.13	0.55	1.06	1.23	1.96	0.99	0.39	0.87	0.55	0.35	0.43	0.11
CaO	51.52	6.82	51.92	9.01	46.56	7.27	53.24	10.48	53.89	4.11	55.55	0.89
K_2O	0.22	0.88	0.09	0.31	1.34	1.64	0.07	1.14	0.06	0.13	–	n.d.
SO_3	1.31	2.70	0.14	0.26	1.46	0.81	1.44	4.65	0.15	0.20	–	n.d.
Cl	0.02	0.07	0.07	n.d.	0.06	0.10	0.01	0.06	–	n.d.	–	n.d.
Total	57.20	1.63	56.95	2.93	61.45	5.28	56.80	1.30	55.37	3.11	55.98	0.98

[a]Ba, Cr, Na, Ni, P, Sr, and Ti were below detection for all analyses. Abbreviations: wt% = mean composition in weight%. s.d. = standard deviation (2σ). n.d. = not determined.

those of Osinski and Spray (2001). It was not possible, using the SEM, to detect any micro-inclusions within the calcite. The ubiquitous presence of SiO_2 in groundmass calcite is, therefore, unusual and difficult to explain due to the charge imbalance it would create in the calcite structure.

Silicate Glass

Impact-generated glass is more common than previously thought (Osinski and Spray 2001), typically comprising ~25–35 vol% of the pale grey crater-fill impactites (Table 1). There is, however, considerable variation in its modal abundance, both within individual samples (e.g., <0.5 to >60 vol% glass) and between different localities (Table 1). In clast-poor regions, silicate glass and calcite are intermingled, but not blended with one another (e.g., Figs. 6c and 6d; cf. Osinski and Spray 2001). No crystallites in the silicate glass have been observed in any of the 90 samples investigated by SEM and optical methods. Similarly, no evidence has been found for reaction or formation of new minerals at the contact between carbonate and groundmass-forming silicate glass. Flow textures and injections of silicate glass into clasts indicate that the silicate phase was originally fluid (Osinski and Spray 2001, 2003).

Seventy-six EDS analyses of silicate groundmass glasses are illustrated in Figs. 7 and 8, with representative analyses given in Table 4. In Fig. 7, it is important to note that there is a large concentration of glass analyses in the Mg-rich triangle (dolomite-quartz-MgO), in contrast to the target rock compositions at Haughton that would predominantly plot in the triangle calcite-dolomite-quartz. The glasses have been subdivided into two main types (G1 and G2) based on a combination of SiO_2 content and oxide totals (Fig. 8). The prefix “G” is used to distinguish these groups of groundmass glasses from glass clasts (“C”) described below. It is notable that Na was below detection limits for all groundmass glasses.

Type G1 glasses are the predominant groundmass-forming glass type. These glasses yield consistently low EDS analytical totals, typically ranging from ~50 wt% to ~65 wt% (Table 4). Based on a comparison of the ratio of C to O peak heights between the glasses and co-existing carbonates and silicates, it appears that the volatile species in these glasses is predominantly CO_2, consistent with the extremely low totals. These glasses are poor in SiO_2 (<40 wt%), FeO (<2.5 wt%), and K_2O (<2.0 wt%) as illustrated in Fig. 8. Al_2O_3, MgO, and CaO contents can be very high (up to ~50, 32, and 29 wt%, respectively), although these oxides display considerable variations (Fig. 8). The binary plots of major element abundances versus SiO_2 for type G1 glasses indicate a negative correlation for CaO and MgO, but no obvious correlation for Al_2O_3, FeO, or K_2O (Fig. 8). SO_3 and Cl are consistently present in trace amounts (up to ~0.5 and 0.4 wt%, respectively) in the majority of type G1 glasses analyzed (Table 4).

Type G2 glasses yield overall higher EDS analytical totals (>80–85 wt%) and higher SiO_2 (~40–55 wt%) and FeO (up to ~6 wt%) contents than type 1 glasses (Fig. 8; Table 4). Type G2 glasses can be further subdivided into two main compositional types (Fig. 8): (a) Al_2O_3-rich (~15–27 wt%), K_2O-rich (~6–12 wt%), MgO-poor (<10 wt%) glasses; and (b) MgO-rich (~15–32 wt%) glasses. These type G2a and G2b glasses represent the most Al_2O_2- and MgO-rich impact glasses, respectively, analyzed at Haughton to date. It is notable that type G2 glasses display no marked correlation of major element abundances versus SiO_2 content (Fig. 8).

Anhydrite

In addition to shock-melted calcite and silicate glass, anhydrite can also constitute an important component of the groundmass (up to ~90%) of the crater-fill impact melt breccias at Haughton (Table 1). Osinski and Spray (2003) found this to be the case in eleven samples from three separate locations. The largest occurrence of anhydrite-bearing impact melt breccias occurs in the basal megabreccia at the base of the crater-fill unit (Figs. 2a and 3). The textural and chemical

Table 2. *Continued*. Average composition of groundmass-forming calcite in crater-fill impactites[a].

Sample #	00-288		02-087		02-088		02-090		02-119		02-133	
Number of analyses	5		3		4		5		4		3	
	wt%	s.d.	wt%	s.d.	wt%	s.d.	wt%	s.d.	wt%	s.d.	wt%	s.d.
SiO_2	0.46	1.05	0.34	0.48	0.38	0.27	0.53	0.63	1.26	3.51	0.14	0.23
Al_2O_3	–	n.d.	0.04	0.19	–	n.d.	0.07	0.27	0.08	0.35	–	n.d.
FeO	0.12	0.22	–	n.d.	0.05	0.21	0.08	0.22	0.04	0.19	0.08	0.41
MnO	–	n.d.	–	n.d.	–	n.d.	–	n.d.	–	n.d.	–	n.d.
MgO	0.56	0.93	0.55	0.26	0.55	0.30	0.62	0.50	0.76	0.62	0.30	0.50
CaO	55.57	2.63	52.41	0.69	52.57	1.25	52.91	1.89	51.95	4.34	54.09	0.64
K_2O	0.05	0.15	0.09	0.11	0.02	0.10	0.06	0.14	0.05	0.13	0.03	0.09
SO_3	–	n.d.	0.04	0.16	0.12	0.48	0.09	0.28	0.26	0.24	0.03	0.16
Cl	–	n.d.	–	n.d.	–	n.d.	–	n.d.	–	n.d.	–	n.d.
Total	56.76	1.22	53.46	0.56	53.69	1.56	54.36	1.20	54.40	1.99	54.68	1.00

[a]Ba, Cr, Na, Ni, P, Sr, and Ti were below detection for all analyses. Abbreviations: wt% = mean composition in weight%. s.d. = standard deviation (2σ). n.d. = not determined.

features of the groundmass-forming anhydrite indicate that this phase, in addition to coexisting carbonates and silicates, crystallized directly from an impact-generated melt (Osinski and Spray 2003). Evidence for this includes: (1) the groundmass-supported nature of the crater-fill lithologies; (2) sulfate-carbonate-silicate liquid immiscible textures; (3) possible quench textures in anhydrite; and (4) flow textures developed between anhydrite and silicate glasses. Further supporting evidence includes the presence of Si (up to ~0.7 wt%) in the anhydrite structure, which was probably "trapped" by quenching from a melt (Osinski and Spray 2003).

Lithic Clasts

Lithic clasts are usually angular and are predominantly carbonates (dolomite >> limestone) (Table 1), the majority of which are either pale grey/white or dark grey/black, in contrast to the brown coloration of the unshocked country rocks (Robertson and Grieve 1978). The crater-fill impact melt breccias appear well-mixed in clast composition and content (Redeker and Stöffler 1988); although, with the bulk of the target sequence consisting of carbonates of similar appearance, this is inherently difficult to quantify. Two sources are, however, particularly easy to recognize as lithic clasts in the field and in thin section: (1) gneisses and metagranites from the Precambrian crystalline basement ("crystalline clasts" in Table 1); and (2) anhydrite and gypsum ("evaporite clasts" in Table 1), predominantly from the Bay Fiord Formation. Crystalline rocks are abundant as clasts in the northeastern sector of the impact melt breccias (cf. Frisch and Thorsteinsson 1978).

Clasts of evaporite-bearing lithologies in the pale grey crater-fill impactites are reported here for the first time. The shocked evaporite lithologies are typically white or pale brown in hand specimen, unlike the unshocked varieties that are typically dark brown. Importantly, evaporite clasts are only present in the eastern half of the crater-fill layer. The large meter-size blocks of Bay Fiord Formation evaporites at the base of the pale grey crater-fill impactites in Fig. 3 are not included in this distinction as these lithologies are unshocked and were probably incorporated during late stage slumping of the transient cavity walls.

Previous workers have carried out detailed studies of the shock features present in crystalline lithic and mineral clasts (i.e., gneisses and metagranites) in the crater-fill impact melt breccias (Metzler et al. 1988; Redeker and Stöffler 1988; Bunch et al. 1998). A detailed study of shock features in the sedimentary clasts is ongoing.

Impact Glass Clasts

Millimeter- to centimeter-size clasts of silicate impact melt glass are present in approximately half the samples studied (Table 1), with no obvious trends in their distribution. Hand specimen-size samples have only been found near the center of the crater at a locality named Anomaly Hill (Fig. 1; cf. Metzler et al. 1988). One hundred and seven EDS analyses of impact glass clasts are illustrated in Figs. 7 and 8, with representative analyses given in Table 5. These glasses can be divided into five main compositional types described below.

Type C1

These are pure SiO_2 glasses with EDS analytical totals >96 wt% and with other major oxides present only in trace amounts (<0.7 wt%) (Fig. 8; Table 5). Type C1 glasses are often intensely vesiculated, with flow textures, and with vesicles ranging from ~1 μm to ~1 cm in diameter (Figs. 9a–c). The highly vesiculated samples are typically white in hand specimen and resemble pumice. They are colorless in transmitted light. Perlitic fractures have been observed in three of the >70 clasts documented (e.g., Fig. 9d). It is of note that none of the type C1 SiO_2-rich glasses at Haughton display the fish-scale pattern known as "ballen" quartz (cf. type C2 and C3 glasses below), that is seen at many other terrestrial impact structures (e.g., Carstens 1975).

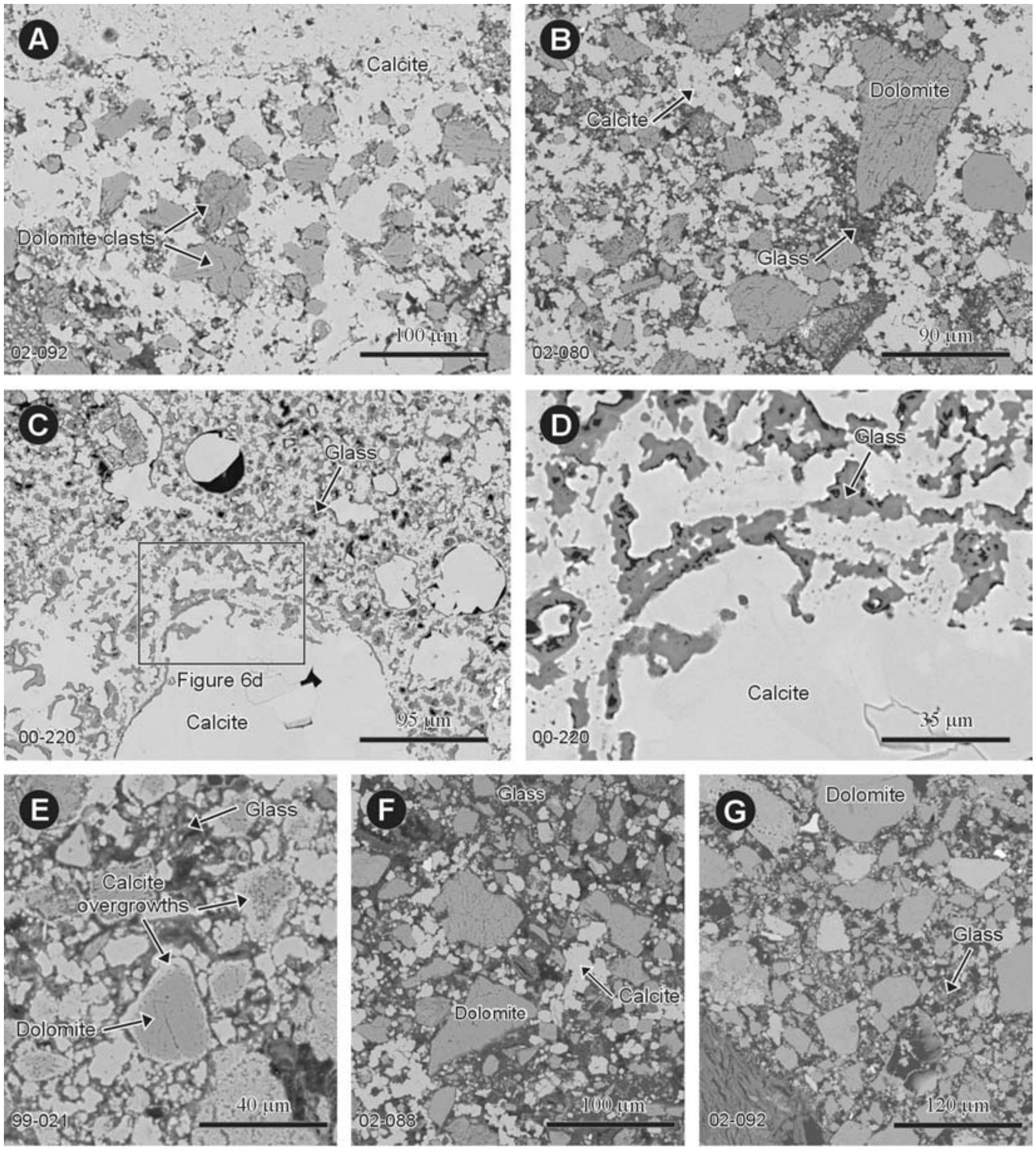

Fig. 6. Backscattered electron photomicrographs showing the progression from calcite-rich to glass-rich areas of the crater-fill deposits. The sample number is shown in the lower left hand corner. a) and b) Shocked dolomite clasts (pale grey) within a predominantly microcrystalline calcite groundmass (white). c) and d) Intergrowth of groundmass-forming calcite (white) and silicate glass (grey). Note the hemispherical void (black) partially mantling calcite spheres (upper center of [c]). This void could be due either to a coexisting vapor phase, or due to a volume change on cooling. e) Calcite (white) overgrowths on shocked dolomite clasts (pale grey), enclosed in silicate glass (dark grey). f) Globules of calcite (white) within a groundmass dominated by silicate glass (dark grey). All of the (sub-) angular pale grey clasts in this image are dolomite. g) Clast-rich region of crater-fill deposits. The clasts are predominantly dolomite (pale grey), with minor quartz (also pale grey), impact melt glass (dark grey at bottom left of image) and pyroxene (small bright white clasts near top of image). The clasts are embedded in silicate glass (dark grey).

Type C2

Type C2 glasses are SiO_2-rich with lower EDS analytical totals (<96 wt%) than type C1 and with other major oxides present only in trace amounts (<0.7 wt%) (Fig. 8; Table 5). The low totals of type C2 glass clasts suggest the presence of substantial amounts of volatiles, which is consistent with their widespread devitrification (Figs. 10a–d). Hand specimen-size clasts of these glasses are typically opaque, cream to pale grey-colored and resemble “flint” in hand specimen. In contrast to all other glass clasts, type C2 glasses lack vesicles. Several samples comprising irregular globular masses and spherulites of these glasses have been observed (e.g., Figs. 10c–d).

It is notable that the more hydrous SiO_2-rich glasses typically contain zoned, subhedral to euhedral crystals of calcite (Figs. 10e and 10f), which are indicative of

Table 3. Average composition of unshocked sedimentary and post-impact hydrothermal calcite phases[a].

Sample #	00-186		99-097		02-087		02-088		99-135		99-079	
Number of analyses	5		8		5		5		10		7	
Description	Clast		Clast		Hyd. vein		Hyd. vein		Hyd. Lam		Undisturbed	
	wt%	s.d.	wt%	s.d.	wt%	s.d.	wt%	s.d.	wt%	s.d.	wt%	s.d.
SiO_2	0.17	0.05	–	–	0.04	0.12	0.02	0.08	0.20	0.48	0.03	0.06
FeO	0.05	0.21	0.04	0.23	–	n.d.	0.02	0.07	–	n.d.	0.12	0.03
MgO	0.39	0.21	0.57	0.43	0.15	0.41	0.51	0.13	0.21	0.28	0.87	0.34
CaO	52.57	1.64	54.03	0.89	53.43	1.20	53.14	1.70	54.73	1.74	52.23	0.98
K_2O	–	–	–	–	–	n.d.	–	n.d.	0.04	0.18	–	n.d.
SO_3	–	–	–	–	0.04	0.17	–	n.d.	–	n.d.	–	n.d.
Cl	0.02	0.10	–	–	–	n.d.	–	n.d.	–	n.d.	–	n.d.
Total	53.17	2.07	54.64	1.74	53.61	1.52	53.69	1.59	55.18	1.51	53.25	1.26

[a]Al, Ba, Cr, Mn, Na, Ni, P, Sr and Ti were below detection for all analyses. Abbreviations: wt% = mean composition in weight%. s.d. = standard deviation (2σ). n.d. = not determined. Hyd. = hydrothermal; Lam. = laminated hydrothermal precipitate.

crystallization from a melt. This observation is in agreement with the fact that the presence of H_2O in a glass increases devitrification rates significantly (Lofgren 1970) and that devitrification accompanies cooling of hot glass and involves the nucleation and growth of crystals at subsolidus temperatures (e.g., McPhie et al. 1993). These calcite crystals can contain up to 8 wt% Al_2O_3 and 2 wt% SiO_2. Importantly, no Al_2O_3 is present in the host glass. Thus, the high Al_2O_3 content cannot be attributed to beam overlap of glass and calcite during EDS analysis (cf. Osinski and Spray 2001).

Type C3

The third glass type is SiO_2-rich (~80–99 wt%) with variable amounts of CaO (~0.5–20 wt%) (Fig. 8; Table 5). These glasses are white in hand specimen and colorless to pale yellow in transmitted light. In some regions of type C3 glass clasts, calcite can comprise >75 vol%, with highly vesiculated glass in the interstitial areas (Fig. 11b). Globules of calcite are a common constituent of these glasses (Figs. 11a and 11b). (Note that glass in close proximity to the globules was avoided during analysis.) There are always sharp and curved menisci between the calcite globules and glass.

Type C4

Glasses with SiO_2 contents of ~40–52 wt%, high MgO contents (up to ~25 wt%), and variable amounts of Al_2O_3 (up to ~12 wt%) and FeO (up to ~8 wt%), represent a fourth glass type (C4). Other major oxides are typically present in traces amounts (<0.5 wt%) (Fig. 8; Table 5). EDS analytical totals for these glasses vary considerably (~70–90 wt%). This compositional glass type (C4) and the last type (C5) are typically dark brown/red in hand specimen and plane polarized light, and less intensely vesiculated than the other three SiO_2-rich glass types described above (Fig. 12).

Type C5

Type C5 glasses are K_2O-rich (~4–10 wt%) with SiO_2 contents typically ~55 to 65 wt%, and variable amounts of Al_2O_3 (up to ~20 wt%), FeO (up to ~4 wt%), and CaO (up to ~4 wt%). EDS analytical totals for type C5 glasses are typically >92 wt% (Fig. 8; Table 5).

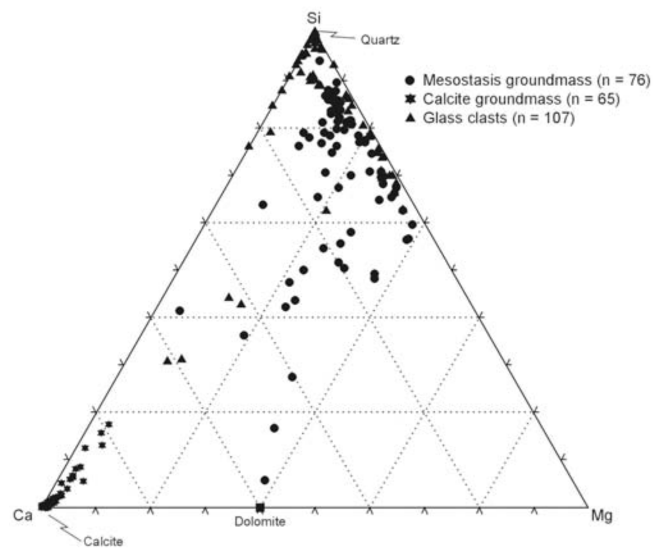

Fig. 7. CaO-MgO-SiO_2 ternary diagram illustrating the relationship between the composition of groundmass-forming calcite and silicate glass, and impact glass clasts from the crater-fill impactites. The plotting parameters were calculated by summing the oxides and recalculating each as a percentage of the sum. Thus, this plot does not use absolute values; however, given that the target sequence at Haughton is dominated by dolomite, calcite, and quartz, this diagram offers a means to compare the varying incorporation of these three minerals into impact-generated melt phases (i.e., calcite and silicate glasses). Note that anhydrite and gypsum would plot at the CaO apex and shales, which are very CaO-MgO-poor, would plot approximately at the SiO_2 apex.

PETROGRAPHY OF IMPACTITES IN THE NEAR-SURFACE CRATER RIM REGION

Two distinct types of allochthonous impactites are present in the crater rim region (Fig. 2): (1) hitherto

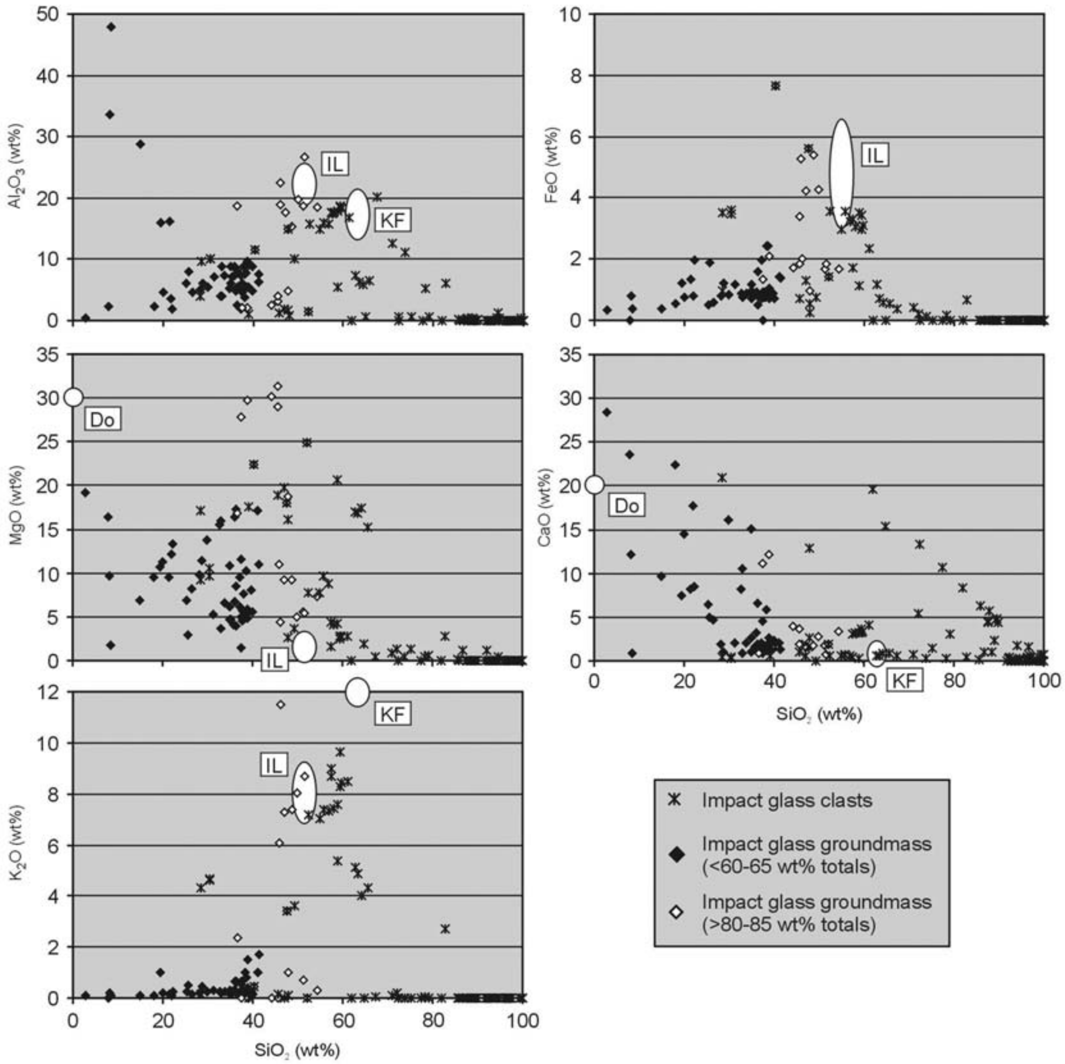

Fig. 8. Harker variation diagrams illustrating individual analyses of groundmass-forming glasses (G1 and G2) and silicate impact melt glass clasts (C1-5) in crater-fill impact melt breccias. The typical compositions of dolomite (Do), potassium feldspar (KF), and illite (IL) are also plotted. Please see the text for a discussion of the relationship between the composition of the impact glasses and the aforementioned minerals. Oxide totals for the various glass types vary considerably so that care must be taken when interpreting any trends. The low totals of many groundmass glasses, in particular type G1, could be due either to poor analyses or to a sub-microscopic porosity. However, if either were the case, the analyses with the lowest oxide totals would be depleted in all elements. This is not the case, as the analyses with the lowest totals typically possess the lowest SiO_2 and the highest CaO-MgO contents, so that the lower totals may reflect the presence of higher amounts of volatiles.

unrecognized impact breccias with a microscopic pale yellow groundmass and pale to dark brown clasts and megablocks; and (2) pale grey impact melt breccias with a microscopic groundmass and with pale grey/white or dark grey/black clasts. The modal abundance in thin section of groundmass and clast types of representative samples from these impactites is given in Table 6. A more detailed description of their characteristics is given below.

Yellow-Brown Impactites

Clasts enclosed in the yellow-brown impactites appear to be from one lithological formation at any particular location (e.g., Fig. 6). As for other impactites from this study, the dominant clast type is dolomite (Table 4). The groundmass consists of microcrystalline calcite and an isotropic SiO_2 phase, which is also typically found devitrified. According to XRD analyses, these devitrified regions consist of α-quartz. XRD analysis of undervitrified regions reveals that the isotropic SiO_2 groundmass phase is a glass. One phase, either calcite or silicate glass, is usually dominant over the other (Table 4). It is notable that the majority of the small calcite bodies in the SiO_2 glass are rounded compared to the larger calcite clasts, which are angular (e.g., Fig. 13a). Clasts set in a calcite groundmass are also angular. Based largely on SEM images, the following textures have been observed: (1)

Table 4a. Representative individual EDS analyses of type G1 groundmass-forming impact melt glasses in the pale grey crater-fill impact melt breccias (wt%)[a].

Analysis #	1	2	3	4	5	6	7	8	9	10	11	12
Sample #	99-001	99-001	99-009	99-015	99-015	99-021	99-021	99-065	00-257	02-090	02-133	02-133
SiO_2	8.27	19.38	21.86	38.54	37.44	32.99	36.18	29.96	36.32	34.94	41.38	39.79
TiO_2	–	–	–	–	–	–	–	–	–	–	–	–
Al_2O_3	33.62	15.95	3.50	7.81	4.65	4.05	4.88	5.45	8.15	6.08	7.60	8.83
FeO	0.81	1.20	0.81	2.45	0.90	0.75	0.88	0.83	1.58	1.17	1.39	0.88
MgO	9.69	10.68	12.23	10.23	11.54	15.94	16.47	13.72	17.31	10.81	11.04	8.02
CaO	12.20	7.48	17.72	1.12	4.53	10.48	3.26	16.17	1.88	1.07	1.30	1.42
K_2O	0.21	1.00	0.11	0.81	0.54	0.19	0.68	0.23	0.64	0.27	1.72	0.25
SO_3	0.42	0.39	0.20	0.22	0.33	0.31	0.25	0.33	0.19	–	0.53	–
Cl	0.33	0.36	0.24	0.39	0.25	0.13	0.10	0.14	0.19	0.22	0.15	0.25
Total	65.54	56.54	56.66	61.56	60.20	64.84	62.70	66.82	66.25	54.57	65.09	59.45

[a]Ba, Cr, Mn, Na, Ni, P, and Sr were below detection for all analyses. Abbreviations: n.d. = not determined.

Table 4b. Representative individual EDS analyses of type G2 groundmass-forming impact melt glasses in the pale grey crater-fill impact melt breccias (wt%)[a].

Analysis #	1	2	3	4	5	6	7	8	9	10	11	12
Sample #	99-001	99-007	99-021	99-044	99-044	00-165	00-165	00-220	00-220	00-220	00-288	00-288
SiO_2	54.24	52.23	40.32	47.15	51.47	46.09	46.01	38.82	44.18	45.53	49.98	36.53
TiO_2	–	–	–	0.62	0.19	0.41	0.31	–	–	–	0.56	0.23
Al_2O_3	18.39	1.37	11.66	17.74	26.68	22.38	18.98	2.09	2.60	3.95	19.74	18.80
FeO	1.69	1.44	7.66	4.23	1.86	2.02	5.25	2.08	1.70	3.39	4.26	13.12
MgO	7.28	24.89	22.43	9.19	5.36	4.45	10.96	29.73	30.17	29.01	4.94	16.84
CaO	3.36	1.89	1.66	1.54	0.70	1.94	1.71	12.12	3.92	1.91	2.74	0.82
K_2O	0.29	–	0.47	7.27	8.67	11.50	6.05	–	–	–	8.03	2.37
SO_3	–	0.33	–	0.42	0.27	0.41	0.17	–	–	–	–	–
Cl	–	0.35	0.08	0.12	–	0.08	0.12	0.33	0.28	0.19	0.17	0.10
Total	85.57	82.49	84.27	88.28	95.20	89.27	89.57	85.16	82.84	83.98	90.42	88.82

[a]Ba, Cr, Mn, Na, Ni, P, and Sr were below detection for all analyses. Abbreviations: n.d. = not determined.

Table 5a. Representative EDS analyses of impact glass clasts from the pale grey crater-fill impact melt breccias (wt%)[a].

Analysis #	1	2	3	4	5	6	7	8	9	10	11	12
Glass type	C1	C1	C1	C2	C2	C2	C2	C3	C3	C3	C3	C3
Sample #	99-069	99-071	99-071	99-069	99-071	00-264	02-119	00-263	00-263	00-263	00-263	00-264
SiO_2	99.98	100.30	100.45	94.47	94.67	96.28	96.81	92.07	89.62	93.94	64.90	81.86
TiO_2	–	–	–	–	–	–	–	–	–	–	–	–
Al_2O_3	–	0.28	–	1.18	–	–	–	–	–	–	0.53	–
FeO	–	–	–	–	–	–	–	–	–	–	–	–
MnO	–	–	–	–	–	–	–	–	–	–	–	–
MgO	–	–	–	–	–	–	–	1.20	–	–	1.94	–
CaO	–	–	–	0.12	–	0.47	0.15	0.32	4.77	5.73	15.34	8.32
K_2O	–	–	–	–	–	–	–	–	–	–	–	–
P_2O_5	–	–	–	–	–	–	–	–	–	–	–	–
SO_3	–	–	–	–	–	–	–	–	–	–	–	–
Cl	–	–	–	–	–	–	–	–	–	–	–	–
Total	99.98	100.65	100.45	95.77	94.67	96.76	96.96	93.59	94.39	99.57	82.71	90.18

[a]Ba, Cr, Na, Ni, and Sr were below detection for all analyses. Abbreviations: n.d. = not determined.

Table 5b. Representative EDS analyses of impact glass clasts from the pale grey crater-fill impact melt breccias (wt%)[a].

Analysis #	13	14	15	16	17	18	19	20	21	22	23	24
Glass type	C4	C4	C4	C4	C4	C4	C5	C5	C5	C5	C5	C5
Sample #	99-065	02-092	02-092	02-092	02-003	00-263	99-065	99-067	99-067	99-067	02-003	02-003
SiO_2	47.75	64.28	63.51	58.79	56.84	47.90	59.36	58.83	61.18	59.31	55.67	82.77
TiO_2	–	0.15	–	–	0.51	–	0.75	0.80	–	0.78	0.57	0.24
Al_2O_3	14.84	5.81	6.34	5.38	15.69	0.83	18.46	17.89	16.73	18.70	15.91	6.17
FeO	5.63	0.61	0.73	1.11	3.24	0.55	2.98	3.53	2.36	3.44	3.57	0.66
MnO	–	–	–	–	–	–	–	–	–	–	0.06	0.05
MgO	18.02	17.40	16.82	20.58	8.76	16.09	2.73	4.19	2.85	2.56	9.60	2.73
CaO	1.67	0.88	0.55	0.36	0.62	12.82	3.24	3.25	4.10	3.60	0.66	0.37
K_2O	3.41	4.02	4.86	5.36	7.31	0.12	8.44	7.58	8.49	9.64	7.37	2.69
P_2O_5	–	–	–	–	0.59	–	–	–	–	–	0.58	0.73
SO_3	–	0.21	–	–	0.35	–	–	–	–	–	0.54	0.73
Cl	0.09	0.14	0.12	0.08	0.33	–	0.25	0.21	0.21	0.36	0.36	0.28
Total	91.30	93.49	92.94	91.65	94.21	78.30	96.07	96.28	95.92	98.39	95.70	98.08

[a]Ba, Cr, Na, Ni, and Sr were below detection for all analyses. Abbreviations: n.d. = not determined.

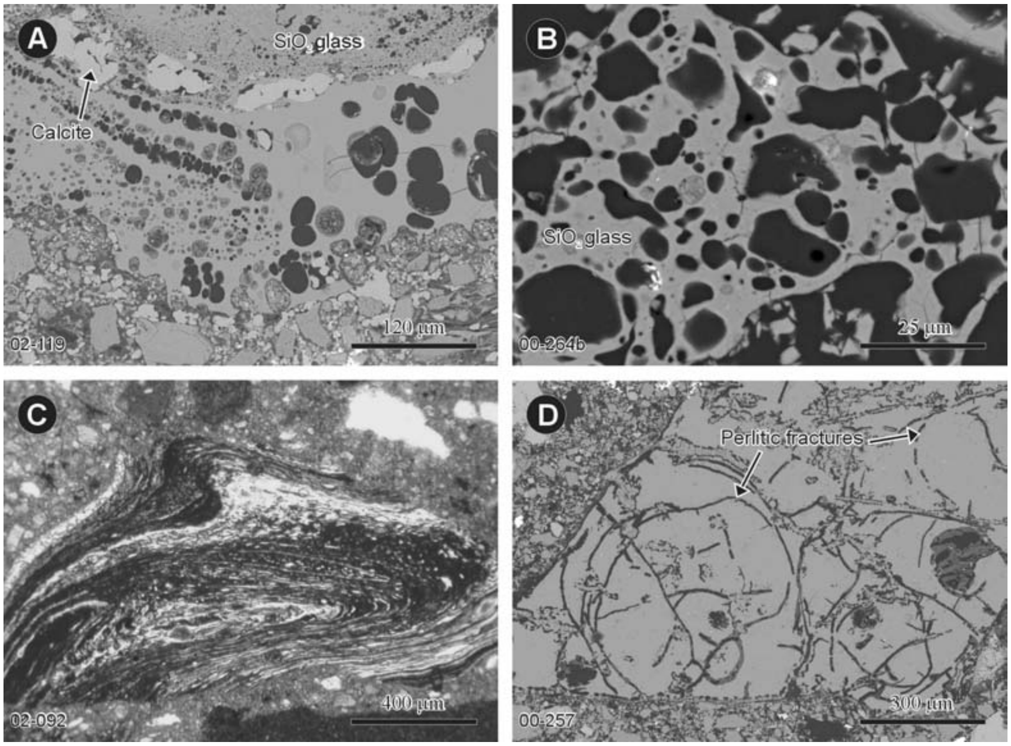

Fig. 9. Backscattered secondary electron SEM images (a, b, d) and plane-polarized light photomicrograph (c) of pure SiO_2 type C1 glasses in crater-fill impact melt breccias. The sample number is shown in the lower left hand corner. (a) Vesiculated glass clast (vesicles appear black) containing globules of calcite (upper three quarters of the image). The pale grey clasts at the bottom of the image are dolomite. b) Intensely vesiculated SiO_2 glass. The vesicles appear black. c) Glass clast with well-developed flow banding enclosed in impact melt breccias. Note that the flow foliations approximately parallel the outline of the clast, suggesting that the glass was (partially) molten during transport. The color banding in the glass clast does not reflect any internal difference in composition. The bright clasts in the upper right of the image are calcite. d) Angular glass clast with well developed perlitic fractures (curved black lines) enclosed in impact melt breccias. Perlitic fractures form due to the accommodation of strain following volume increases associated with the diffusion of meteoric water into the solid glass (Marshall 1961).

individual calcite spheres and globules within SiO_2 glass and vice versa (e.g., Figs. 13b and 13c); (2) intermingling, but not blending, of calcite with SiO_2 glass; (3) coalesced, or partially coalesced SiO_2 glass globules and blebs within silicate glass; and (4) curved menisci with sharp boundaries between silicate glass and calcite (e.g., Fig. 13c). Small (<15 µm long) skeletal laths of pyrite are present in groundmass-forming impact melt glass (e.g., Fig. 13d).

Pale Grey Impact Melt Breccias

The pale grey impact melt breccias of the crater rim area resemble the crater-fill impact melt breccias in hand specimen; however, there are important differences. Firstly, the groundmass of these impactites is dominated by calcite (up to ~60 vol%), with impact melt glass comprising <10 vol%, and anhydrite absent (Table 4). By analogy with the crater-fill impact melt breccias, the calcite and impact glass in the groundmass of these impactites also have an impact melt origin (cf. Osinski and Spray 2001).

Secondly, the modal abundance and composition of clasts (Table 4) are totally different than for the crater-fill impact melt breccias (Table 1). Dolomite clasts are the dominant type in both field settings, but limestone clasts are slightly more abundant in the crater rim impact melt breccias (up to ~15 vol%) (Table 4). Evaporites and sandstones are rare (<2 vol%) as clasts in thin section and in hand specimen. No lithic or mineral fragments from the crystalline basement, or impact glasses, have been observed in thin section (Table 4). The inspection and classification of >1000 hand specimen-sized clasts in the field yielded only three small (<2 cm in diameter) crystalline clasts. These crystalline clasts were not in situ and are so small and rare, that it cannot be ruled out that they have been transported considerable distances, either by aeolian, glacial, or fluvial processes.

DISCUSSION

Origin of Groundmass Phases of Crater-Fill Impact Melt Breccias

Textural and chemical evidence presented here, together with that previously documented by Osinski and Spray (2001, 2003) indicate that groundmass-forming calcite, silicate glass,

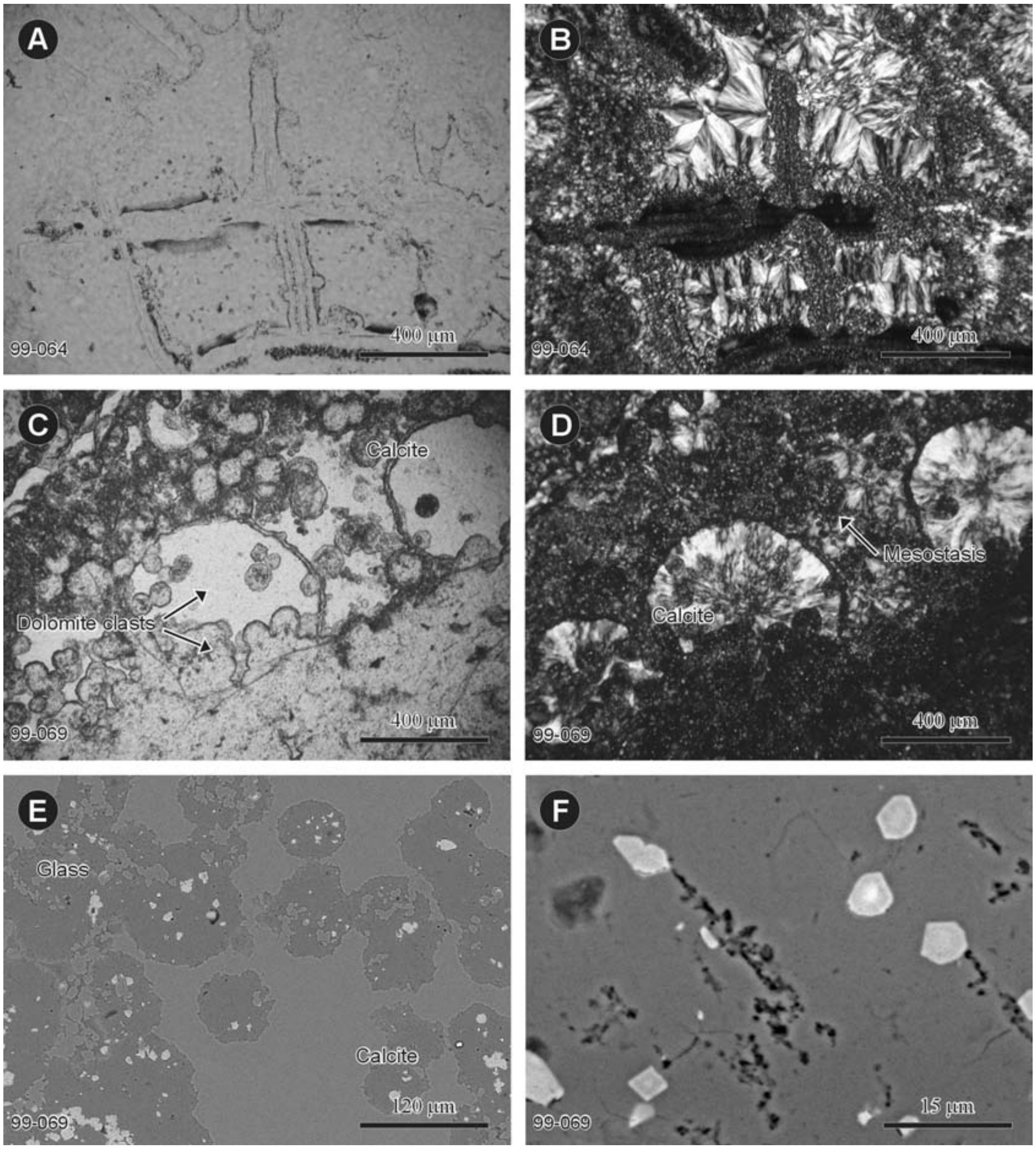

Fig. 10. Optical photomicrographs (a–d) and backscattered secondary electron SEM images (e and f) of type C2 glasses in crater-fill impact melt breccias. The sample number is shown in the lower left hand corner. a) and b) Images of the same region of a polished thin section in plane- and cross-polarized light showing the typical devitrified nature of type C2 glasses. c) and d) Plane- and cross-polarized light photomicrographs, respectively, of the same region of a polished thin section showing two varieties of SiO_2-rich type C2 glasses. The first variety (I) consists of large, originally glassy, spherulites that have devitrified to quartz. These appear colorless in plane-polarized light (c) and display a radiating texture in cross-polarized light (d). These spherulites enclose smaller, coalesced globular masses of glass (II). e) Backscattered secondary electron SEM image showing a close-up of the two varieties of type C2 glass shown in (c) and (d). The globular masses (glass variety II) are rich in H2O-rich (~8–10 wt%; as revealed by EDS analysis) and contain abundant microscopic calcite crystals. f) Close-up view of globular glasses showing the well-developed euhedral form of the zoned calcite crystals. EDS analyses reveal that these calcites can contain up to ~7 wt% Al_2O_3 and ~2 wt% SiO_2. Given that the enclosing glass is pure SiO_2 (+H_2O), the Al_2O_3 has clearly been incorporated into the calcite.

and anhydrite of the pale grey impactites in the interior of the Haughton impact structure are all primary impact melt phases.

The relatively higher MgO, FeO, SiO_2, and Al_2O_3 contents of the groundmass-forming calcite contrast with calcite phases analyzed in unshocked/shocked sedimentary clasts and post-impact hydrothermal products at Haughton. Carbonatitic (i.e., igneous) calcites are the only known examples to contain elevated levels of SiO_2 and Al_2O_3. Indeed, all carbonatite melts contain silicate components in solution (typically >5 wt% SiO_2) (Bell et al. 1998), with the solubility of SiO_2 in the melt increasing with increasing temperature (e.g., Brooker 1998). Rapid crystallization (quenching) of a high temperature SiO_2-rich carbonatite melt

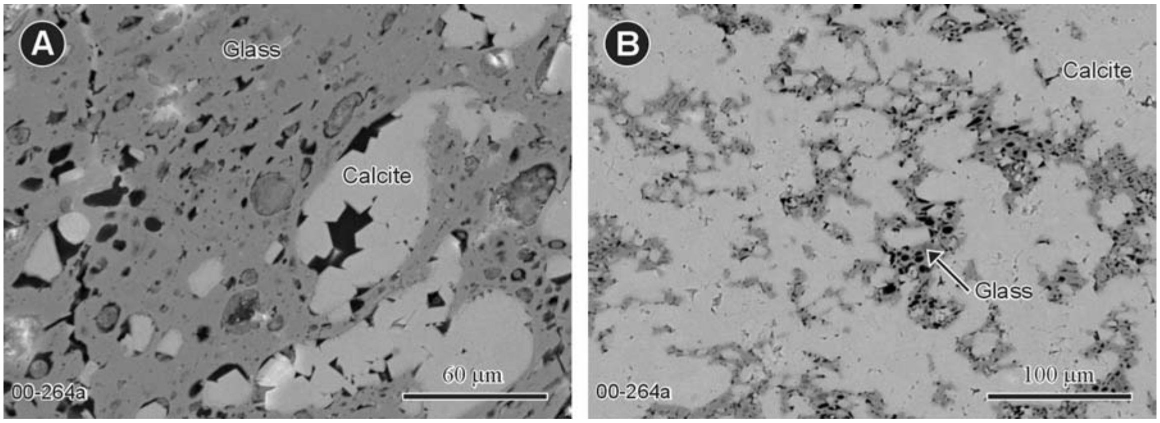

Fig. 11. Backscattered secondary electron SEM images of the same SiO_2-rich type C3 glass clast showing the varying proportion of calcite. The sample number is shown in the lower left hand corner. a) The bulk of the image consists of vesicular glass (pale grey), with isolated globules of calcite (white). Note the presence of a void (black) in the center of the large calcite globule (right of center). This void can be explained either as the result of a coexisting vapor phase, or due to a volume change on crystallization of the calcite. b) In regions of the glass clast where calcite dominates, the glass (pale grey) is restricted to highly vesiculated schlieren between the larger calcite masses.

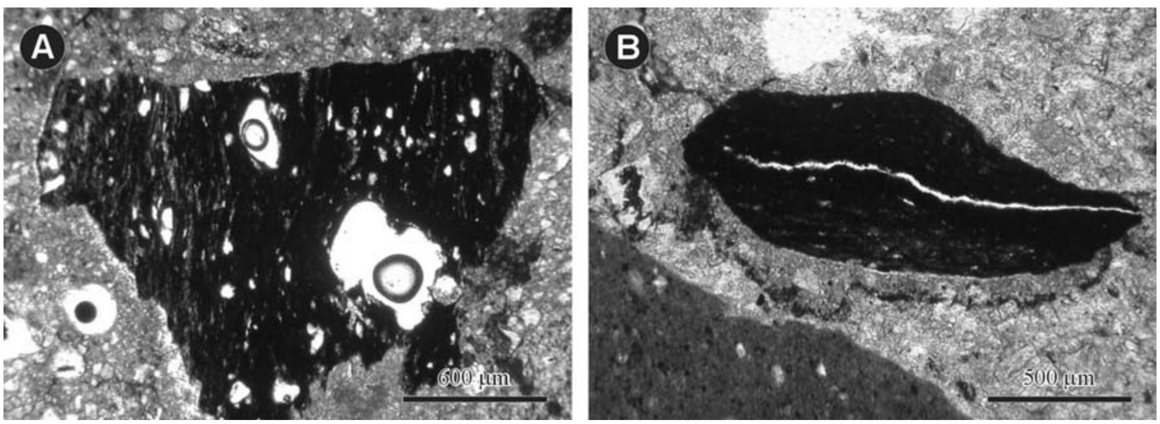

Fig. 12. Plane-polarized light photomicrographs of types C4 (a) and C5 (b) impact glasses. The sample number is shown in the lower left hand corner. Both these clasts appear dark brown-red in plane- and cross-polarized light. The sample number is shown in the lower left hand corner. In detail: a) Image of a flow-textured type C4 glass clast surrounded by the fine-grained groundmass of the crater-fill impact melt breccias. The flow foliations can be seen trending sub-vertically in the glass clast. The bright white "globules" in the glass clast are vesicles. whereas in the groundmass, they represent regions where clasts have been plucked out during thin section preparation. b) Type C5 glass clast displaying faint flow banding trending sub-horizontally across the image. The large dark object in the lower left of the image is a dolomite clast.

Table 6. Modal composition of impact melt breccias of the crater rim area (vol%)[a].

	UTM position		Groundmass						Clasts				
Sample	Easting	Northing	Cal	Gls	An	Tot	Dol	Lst	Evp	Sst	Xst	Gls	Tot
Pale grey-weathering impact melt breccias													
00-165	418,560	8,363,170	51.0	8.1	–	59.1	39.0	1.9	–	–	–	–	40.9
00-167	418,560	8,363,170	53.4	4.7	–	58.1	27.4	13.3	1.0	0.2	–	–	41.9
00-171	418,620	8,363,230	49.6	9.9	–	59.5	29.2	9.5	1.5	0.3	–	–	40.5
01-035	418,650	8,363,210	59.9	4.5	–	64.4	23.2	12.3	–	0.1	–	–	35.6
Pale yellow impact melt breccias													
00-186	418,920	8,364,550	9.2	67.1	–	76.3	22.9	0.8	–	–	–	–	23.7
00-187	418,920	8,364,550	46.3	13.5	–	59.8	38.3	1.9	–	–	–	–	40.2

[a]Abbreviations: Cal = calcite; Gls = silicate impact melt glass; An = anhydrite; Tot = total; Dol = dolomite; Lst = limestone; Evp = evaporite (gypsum and/or anhydrite); Sst = sandstone; Xst = crystalline.

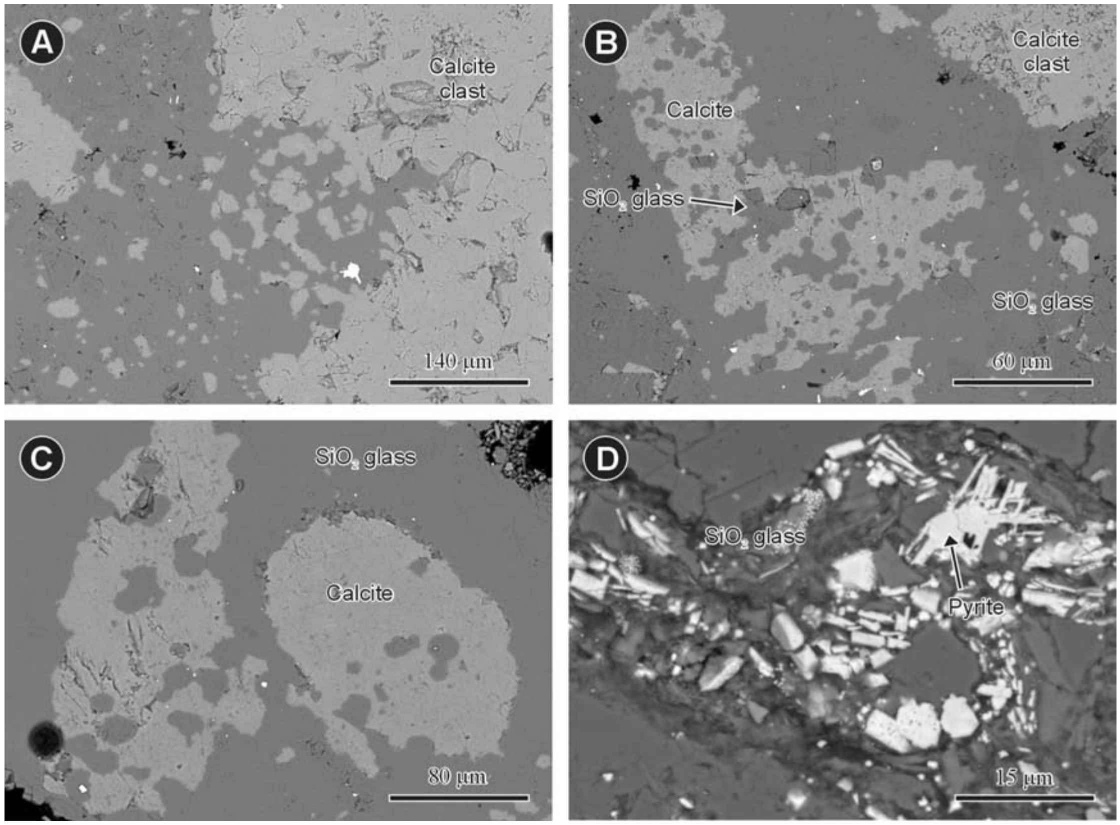

Fig. 13. Backscattered secondary electron SEM images of yellow-brown impact melt breccias from the near-surface crater rim region. The sample number is shown in the lower left hand corner. a) Irregularly shaped blebs of calcite (pale grey-white) and a large angular clast of calcite (right side of image) in a groundmass of SiO_2 glass (dark grey). b) and c) Globules of calcite within SiO_2 impact glass and vice versa. This indicates that the two phases were originally immiscible liquids. The fact that the larger clasts of calcite retain an angular outline suggests that the smaller calcite globules underwent (partial) melting in the SiO_2 liquid phase. d) Acicular and rare skeletal laths of pyrite (bright white) in a groundmass of SiO_2 impact glass (dark grey).

can, therefore, produce relatively SiO_2-rich carbonates (e.g., carbonates with ~3–10 wt% SiO_2 were produced in the experiments of Brooker 1998). This compositional data provides further evidence for the impact melt origin of calcite in the groundmass of the pale grey crater-fill impactites at Haughton. It is, however, not clear if the Si and Al is incorporated into the calcite structure or if Si and/or Al is present in nanometer-size silicates that crystallized from the $CaCO_3$-rich melt during quenching.

It is notable that a large proportion of silicate glass analyses plot in the Mg-rich triangle dolomite-quartz-MgO in Fig. 7. At first glance, this may seem surprising, since the target rocks at Haughton are dominated by carbonates (~75–80%), with minor evaporites, quartz sandstones, and shales. In other words, there is a relative enrichment of MgO in the silicate glasses. By way of explanation, it is apparent from studies of carbonatites (e.g., Fanelli et al. 1986; Harmer and Gittins 1997) and from previous studies at Haughton (Osinski and Spray 2001) that calcite can precipitate from a dolomitic melt. Indeed, the phase relations of the systems CaO-MgO-CO_2-H_2O (Lee et al. 2000) and CaO-MgO-SiO_2-CO_2-H_2O (Otto and Wyllie 1993), indicate that calcite is the liquidus phase for a wide range of compositions and pressure-temperature conditions. Thus, even if dolomite-rich target rocks are shock melted, calcite is typically the first phase to crystallize out of the melt, with dolomite only forming at lower temperatures upon slow cooling, which, given the rapid quenching of many impact melts may be a rare occurrence. Crystallization of calcite will, therefore, lead to an enrichment of MgO in the residual melt. At Haughton, this residual MgO-enriched melt quenched to a glass before dolomite crystallization could occur.

Silicate glasses in the groundmass of the pale grey crater-fill impact melt breccias are unusual in yielding consistently low totals during EDS analysis. Totals range from ~50 to ~65 wt% in type G1 glasses and ~80 to 95 wt% in type G2 glasses. The low totals of these glasses could be due either to poor analyses or to a sub-microscopic porosity. However, if either were the case, type G1 glasses should be depleted in all elements compared to type G2 glasses. This is not the case, as type G1 glasses are commonly enriched in certain oxides (e.g., CaO and MgO) relative to type G2 glasses (Fig. 8). Thus, the low totals may reflect the presence of high amounts of volatiles in the groundmass glasses. This is consistent with experiments on carbonatites systems, which show that CO_2 solubility in melts increases with decreasing SiO_2 content (Mysen et al. 1975; Mysen 1976; Brooker et al. 2001). A final possibility to be considered is that the groundmass silicate glasses may be hygroscopic (i.e., they can take up H_2O from the atmosphere), which would lead to a further increase in volatile content and a lowering of oxide totals during EDS analysis.

Implications and Comparison with Other Impact Sites

This work has extended the previous studies of Osinski and Spray (2001, 2003) and indicates that the groundmass for the entire pale grey crater-fill unit (i.e., not just isolated samples) has a primary impact melt origin. Thus, these impactites can be classified as impact melt breccias or clast-rich impact melt rocks, according to the terminology of Stöffler and Grieve (1996). They are not clastic matrix breccias or fragmental breccias as previously thought (e.g., Redeker and Stöffler 1988), nor are they “suevitic breccias” as postulated by Dressler and Reimold (2001), or “suevites” as recently inferred by Schmitt et al. (2004). This should not be as surprising as it might appear, as the crater-fill deposits at Haughton are stratigraphically equivalent to coherent impact melt sheets developed at craters in crystalline targets (cf. Grieve 1988). Furthermore, the present and probable original volume (~7 km^3 and ~22.5 km^3, respectively), the stratigraphic succession upwards from target rocks into impact melt breccias, and the relatively homogeneous distribution of clasts, are all analogous to characteristics of coherent impact melt sheets developed in comparably sized structures formed in crystalline targets. Detailed field studies reveal that lithic breccias (i.e., comprising a clastic matrix/groundmass) do occur underlying the impact melt breccias (Fig. 2); however, they are typically discontinuous and a few meters thick at most. Similar observations of lithic breccias underlying impact melt lithologies have been documented in many impact structures developed in crystalline targets (e.g., the Mistastin impact structure, Canada; Grieve 1975).

It is apparent from this study that the clast content of crater-fill impact melt breccias at Haughton (up to ~40–50 vol%) (Table 1) is higher than in comparably sized structures developed in crystalline targets (e.g., ~20–30 vol% at Mistastin; Grieve 1975). It is suggested that this may be explained by the effect of mixing “wet” sediments or carbonates into a melt as opposed to dry crystalline rocks. Kieffer and Simonds (1980) note that the enthalpies of H_2O-bearing and carbonate systems are so high that a much smaller proportion of admixed sedimentary rocks than of anhydrous crystalline rock is required to quench the melt to subsolidus temperatures. Thus, all other conditions being equal, a lower percentage of sedimentary rocks will be assimilated than crystalline rocks, before a melt is quenched. This phenomenon will also result in higher final clast contents for melts derived from impacts into sedimentary as opposed to crystalline targets.

Origin of Groundmass Phases and Classification of Impactites of the Near-Surface Crater Rim Region

Pale grey impactites in the crater rim region comprise a calcite-silicate glass groundmass similar to that of the pale grey impactites in the crater interior. By analogy with the crater-fill impact melt breccias, all groundmass phases within the impactites of the crater rim region have an impact melt origin. The yellow-brown impactites of the crater rim area comprise a microscopic groundmass of microcrystalline calcite and SiO_2 glass, which typically is devitrified. The SiO_2 glass is unequivocally shock-melted. There is abundant evidence for liquid immiscible textures between SiO_2 glasses and calcite (Fig. 13), indicating that both phases were in the liquid state at the same time at high temperatures (>1986 K, the melting point of pure quartz). Based on the arguments above, both types of impactites found in the near-surface crater rim region can be classified as impact melt breccias or clast-rich impact melt rocks, according to the terminology of Stöffler and Grieve (1996).

Initial Temperature and Cooling Rate of Sediment-Derived Impact Melts at Haughton

It is known that impact melt derived from crystalline rocks is superheated with initial average temperatures on the order of ~2000–2500 K (see Grieve et al. 1977 and references therein). The presence of SiO_2-rich glasses derived from sandstones at a number of terrestrial impact structures (e.g., Gosses Bluff [Milton et al. 1996]; Ries [Osinski 2003]), would suggest initial textures of >2000 K. Complications arise as it known that the energy deposited by the passage of the shock wave can be focused in to, and around, pore spaces in sandstones, which results in very localized high pressures and temperatures that can melt quartz within a few micrometers of the pore space, but not in the surrounding grains (Kieffer 1971; Kieffer et al. 1976). However, many of the SiO_2 glass clasts at the Ries impact structure are centimeter-sized (Osinski 2003), while the Gosses Bluff glasses form the groundmass of impact melt breccias (Milton et al. 1996) (i.e., these glasses do not represent localized melts). This suggests that the average initial temperatures of these particular sandstone-derived melts were on the order of ~2000 K.

By analogy, the presence of immiscible textures between calcite and SiO_2 glass at Haughton indicates post-shock temperatures of >2000 K for the carbonate-rich impact melt breccias. The glassy nature of the silicate phases and the absence of crystallites in the groundmass glasses in the Haughton impactites indicates subsequent rapid cooling below the liquidus for these melts (~900–1200 K). The presence of rare larnite (Ca_2SiO_4) and pigeonite in impact glass clasts (Martinez et al. 1994), attests to very minor crystallization at temperatures >1200 K. The rapid quenching of the sediment-derived impact melts at Haughton is also consistent with their extreme chemical heterogeneity, their disaggregated nature (i.e., a coherent melt sheet did not form), the lack of primary dolomite (see previous section), and the lack of reaction between carbonates and silicates.

Crater-Fill Impact Melt Breccias: Depth and Stratigraphic Location of Melting

Evidence from Impact Glass Clasts

Impact glasses can yield valuable information on the depth and stratigraphic location of melting at an impact site. Impact glass clasts within the crater-fill impact melt breccias at Haughton have been divided into five main compositional and textural types (C1 to C5) (Table 5). The only possible protolith for the three SiO_2-rich (>80 wt%) glasses (C1 to C3) are sandstones. Sandstones are restricted in occurrence to lower levels of the sedimentary cover sequence, being most prevalent in the Blanley Bay (>1320 to <1430 m depth) and Cass Fiord (>1560 to <1590 m depth) formations, and the lowermost sedimentary units overlying the crystalline basement (>1840 to <1880 m depth) (Fig. 1c). Types C2 and C3 glass clasts contain substantial amounts of CaO (up to ~20 wt%) and/or globules of calcite and/or euhedral, zoned calcite crystals. These latter two glass types are consistent with the impact melting of calcite-cemented sandstones that are common in the lowermost part of the Paleozoic sequence, and which are present as clasts within the impact melt breccias.

The totals of type C4 glasses vary considerably (~70–90 wt%), suggesting variable amounts of volatiles. This requires a component of carbonate in the melt zone for these glasses. High MgO contents in type C4 glasses indicate a dolomite-bearing protolith; whereas, the high Al_2O_3 and FeO contents suggest a clay-rich input. Illite is the most common clay mineral in the sedimentary succession at Haughton (Thorsteinsson and Mayr 1987). Minor amounts of shales and clay-rich horizons are present throughout the sedimentary sequence but are typically only a few centimeters thick. As with sandstones, shales are most common in the lowermost part of the sedimentary succession, particularly in the Cass Fiord Formation at a depth of ~1620–1680 m (Fig. 1c). The final type (C5) of impact glasses are K_2O-rich varieties (~4–10 wt%), suggesting an origin through the impact melting of potassium feldspar and/or illite-bearing sedimentary rocks. Potassium feldspar is a common detrital and/or authigenic phase in most of the carbonates in the target sequence.

Evidence from Groundmass Phases

The groundmass of the pale grey crater-fill impact melt breccias comprises microcrystalline calcite, silicate impact melt glass, and anhydrite. Given that calcite can precipitate from a dolomitic melt and that carbonates form ~75 vol% of the target sequence at Haughton, little can, therefore, be said about the depth of origin for the calcite component of the groundmass of the crater-fill impact melt breccias.

Two main compositional types (G1 and G2) of glass have been recognized in the groundmass of crater-fill impact melt breccias. The bulk of the groundmass-forming glasses yield very low EDS analytical totals (~50–65 wt%), consistent with high contents of CO_2, suggesting that an origin by the impact melting of carbonates in the sedimentary sequence at Haughton. This is supported by the overall increase in CaO and MgO contents with decreasing SiO_2 content (Fig. 8). Given the high MgO contents (up to ~35 wt%) of many of the groundmass glasses, dolomite (~21 wt% MgO and ~31 wt% CaO) must have been a major component in the source region for the groundmass glasses (Fig. 8). It is notable that groundmass glasses with high CaO contents are rare (Fig. 8). This could be due to the lack of limestones in the melt zone; however, as noted earlier, it appears that calcite can precipitate from a dolomitic melt, so that CaO will be depleted in the residual "glass." Thus, it is not possible to quantify the relative proportions of dolomite versus limestone involved in the formation of these glasses.

The SiO_2 content of the groundmass glasses varies from ~5 up to ~55 wt%. This correlates well with the variable amount of quartz (up to ~25%) in the majority of dolomites in the sedimentary target sequence (Thorsteinsson and Mayr 1987). As the crater-fill impact melt breccias enclose shock-melted clasts of sandstone and shale, SiO_2 could also be derived from minor amounts of these lithologies incorporated in the melt zone. This would also account for the high content of Al_2O_3 and low, but persistent amounts of FeO and K_2O (both typically <2 wt%) (Fig. 8), present in the groundmass glasses.

The origin of primary anhydrite in the groundmass of crater-fill impact melt breccias is easier to constrain. The major evaporite horizons in the target sequence at Haughton occur in the ~290 m thick Bay Fiord Formation, the base of which is at a pre-impact depth of ~1050 m (Fig. 2). The basal ~55 m thick section of the formation consists of anhydrite and minor secondary gypsum (Thorsteinsson and Mayr 1987). Minor amounts of anhydrite are also found in older sedimentary units (Thorsteinsson and Mayr 1987); however, the total amounts are negligible (few meters thickness in total). Thus, it appears that evaporites from pre-impact depths of >920 to <1050 m were incorporated into the melt zone at Haughton.

Synthesis

The evidence from groundmass phases, and from individual glass clasts, suggests that a substantial proportion of the sedimentary sequence underwent melting during the Haughton impact event to form the crater-fill impact melt breccias. Impact glass clasts preserve unequivocal evidence for the impact melting of shales, quartz sandstones, and carbonate-bearing sandstones. The high MgO content of many of the glasses (groundmass phases and clasts) also indicates that dolomite-bearing lithologies underwent melting, as dolomite is the only Mg-rich phase in the sedimentary target sequence. The notable absence of any $CaCO_3$ or $CaMg(CO_3)_2$ glasses at Haughton is consistent with observations from field studies of carbonatites and from melting experiments, in which Ca- and Mg-carbonate glasses have never been observed, and are not expected to form (Barker 1989). This is due to the ionic nature of carbonate melts (Treiman 1989), which leads to their crystallization, even during the most rapid quenching.

Thus, it is apparent that the melt zone incorporated a substantial part of the lower sections of the sedimentary sequence (i.e., carbonates, sandstones, and shales, at depths of >1300 to <1880 m) (Fig. 1c). This is also consistent with recorded peak shock pressures in the crystalline basement of ~80 GPa (Bunch et al. 1998). The impact melting of evaporites indicates that the melt zone also incorporated evaporites at depths of >920 to <1050 m (Fig. 1c).

Impactites of the Crater Rim Region: Depth and Stratigraphic Location of Melting

The evidence suggesting that the pale grey weathering impact melt breccias of the crater rim region were derived from a limestone-rich source region includes: (1) the predominance of calcite as a groundmass phase (i.e., the groundmass is Mg-Si-Al-Fe-poor compared to the crater-fill impact melt breccias); and (2) the predominance of carbonate clasts, the majority of which are either limestone or dolomitic limestone. At Haughton, limestones are predominant at depths of >520 to <750 m and >1050 to <1300 m (Fig. 1c).

The second type of impactite in the crater rim region has a pale yellow groundmass dominated by calcite with varying amounts of SiO_2 glass. The clast population of these impact melt breccias varies considerably between different localities, but is fairly uniform at individual sites. This suggests that these impactites were derived from specific regions of the evolving crater. At two sites, the majority of clasts could unequivocally be assigned to the Thumb Mountain Formation (>680 to <760 m) (Fig. 1c) and the Middle Member of the Allen Bay Formation (>200 to <500 m) (Fig. 1c), respectively. This suggests that the yellow-brown impact melt breccias (i.e., melt component and clasts) of the crater rim region are most likely derived from the upper few hundred meters of the target sequence.

Origin and Emplacement of Allochthonous Impactites at Haughton

Crater-Fill Impact Melt Breccias

Redeker and Stöffler (1988) considered the emplacement of the crater-fill impact melt breccias to be basically airborne, drawing analogies with the crater-fill suevite at the Ries impact structure, Germany. Implicit in this interpretation is that the groundmass/matrix component of these rocks has been considered to be completely clastic/fragmental and lacking in impact melt phases (Redeker and Stöffler 1988). However, Grieve (1988) suggested that while this may be so, there was also a likely component of radial outflow that incorporated material from beyond the volume close to the point of impact. Grieve (1988) cited two main reasons for this: (1) the heterogeneous distribution of crystalline basement clasts in the crater-fill; and (2) the presence of less shocked, including unshocked, mineral grains compared to the recorded shock levels in clasts of their source rocks (Metzler et al. 1988; Redeker and Stöffler 1988). To this list should be added the heterogeneous distribution of evaporite clasts in the crater-fill impact melt breccias.

Based on the observation that the groundmass of the pale grey crater-fill deposits at Haughton represents a series of impact-generated melts, it is proposed that these impactites formed by radial outflow within the transient cavity and were, therefore, never airborne (cf. Grieve 1988). In this respect, it is believed that the pale grey crater-fill impact melt breccias at Haughton formed in the same manner proposed for crater-fill impact melt rocks in crystalline targets (i.e., the model of Grieve et al. 1977). This supported by the similar spatial distribution, stratigraphic succession, and volume of the crater-fill impact melt breccias at Haughton, with characteristics of coherent impact melt sheets in comparably sized structures formed in crystalline targets (cf. Grieve 1988). A detailed cratering model for the Haughton impact event is presented in Osinski et al. (2005).

Impact Melt Breccias of the Near-Surface Crater Rim Region

Two principal impactites have been recognized in the near-surface crater rim area of Haughton (from the base upwards): (1) pale yellow impact melt breccias and megablocks derived from the uppermost part of the target sequence; and (2) pale grey impact melt breccias, derived from deeper levels of the pre-impact stratigraphy. It is notable that the same stratigraphic sequence of impactites in the crater rim area occurs at the Ries impact structure (e.g., Pohl et al. 1977). The pale yellow impact melt breccias and megablocks at Haughton occur in the exact same stratigraphic position as the Bunte Breccia at Ries, which is widely accepted to be a continuous ballistic ejecta deposit (Oberbeck 1975; Morrison and Oberbeck 1978; Hörz et al. 1983). By analogy, we interpret the pale yellow impact melt breccias and megablocks at Haughton as remnants of the continuous ejecta blanket. This is supported by the observation that clasts and megablocks in these deposits are typically highly polished, with well-developed lineations, a feature also seen at Ries and implying ballistic ejection. In addition, the shallow origin (>200 to <760 m) of these deposits is also consistent with an ejecta origin (Fig. 14). Importantly, this constrains the depth of excavation at Haughton to a maximum of ~700–800 m.

An important difference between the Bunte Breccia and the ejecta at Haughton is the presence of impact melted materials in the latter. However, these agree with current

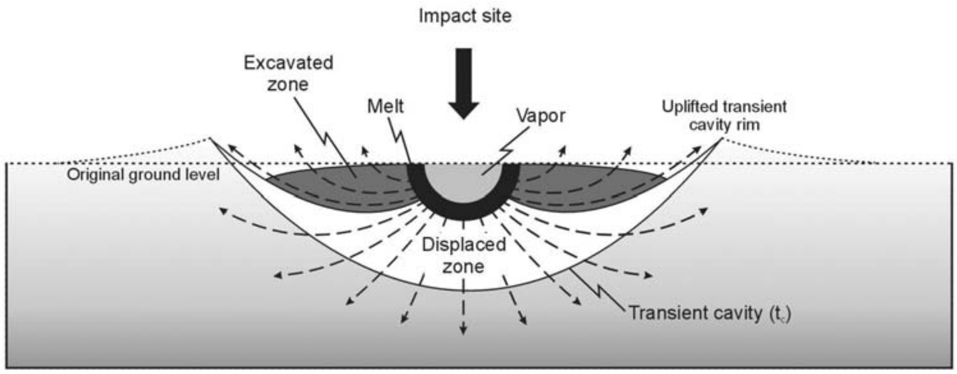

Fig. 14. Theoretical cross-section through a transient cavity showing the locations of impact metamorphosed target lithologies. Excavation flow lines (dashed lines) open up the crater and result in excavation of material from the upper one-third to one-half the depth of the transient cavity. Modified after Grieve (1987) and Melosh (1989).

models for the impact process, which predict that impact melt should be ejected during the excavation and formation of the transient cavity (Fig. 14). As Melosh (1989) notes, "even the lowest velocity ejecta will contain some highly shocked impact melt." Thus, cratering models and the evidence from Haughton would suggest that impact melt phases should be present in ejecta at the majority of impact sites.

We turn now to the origin of the pale grey impact melt breccias that overlie the ejecta deposits at Haughton, and which occur in the same stratigraphic position as surficial (or "fallout") suevites at the Ries structure. The main locality in the southwest of the Haughton structure has not been studied before, so it is not clear if previous workers considered these impactites to be emplaced in an airborne fashion similar to that proposed for the impactites of the crater interior at Haughton and the Ries suevites (Redeker and Stöffler 1988).

For reasons outlined below, we propose that the pale grey impact melt breccias in the crater rim area at Haughton were emplaced in the form of an impact melt-rich flow(s) with entrained clasts:

1. The lack of sorting in these impactites is not predicted by subaerial deposition from an ejecta plume, as those deposits are typically well-sorted and display normal grading, as is the case in pyroclastic fall deposits (e.g., Fisher and Schmincke 1984).
2. The calcite and silicate glass of the groundmass of these impactites represent a series of impact-generated melts that were molten at the time of, and after, deposition. In any model that involves some component of ballistic ejection and transport through the atmosphere, silicate melt would be quenched to a glass before deposition and carbonate melt would have crystallized (e.g., the feathery-textured carbonates in ejecta at the Chicxulub impact structure, Mexico; Jones et al. 2000).
3. Keeping in mind the first two reasons, the stratigraphic relationship between the pale grey impact melt breccias and the underlying ejecta (pale yellow impact melt breccias) at Haughton is consistent only with an impact melt flow origin for the former. It has been documented by many workers that exterior impact melt deposits typically overlie the continuous ejecta deposits of lunar craters (e.g., Howard and Wilshire 1975; Hawke and Head 1977). These features indicate that most of the exterior melt flows were emplaced during the modification stage of complex crater formation (cf. Hawke and Head 1977).
4. As noted, the pale grey impact melt breccias at Haughton lie in the same stratigraphic position as surficial suevites at the Ries. The Ries suevites have recently been reinterpreted as clast-rich impact melt flows (Osinski et al. 2004). By analogy, and based on the evidence presented in this work, these observations strongly suggest that the Haughton pale grey impact melt breccias originated as impact melt-rich flows, that were emplaced outwards from the crater center during the modification stage of crater formation.

CONCLUSIONS

Our studies have revealed the presence of a similar succession of impactites at Haughton as at complex impact structures developed in crystalline target rocks (e.g., Mistastin and Manicouagan). Impact melting and the generation of impact melt rocks during hypervelocity impact into sedimentary targets, therefore, appears to be more common than previously thought. The lithological products of impact into sedimentary targets (e.g., the pale grey impact melt breccias at Haughton) may appear very different from those developed in crystalline targets (e.g., coherent sheets of impact melt rocks with classical igneous textures and features). However, the use of the SEM for microscopic imaging and analysis suggests that these different lithologies may be genetically equivalent.

This work also provides valuable insights into the response of carbonates to hypervelocity impact. In particular, at Haughton, the dominant process was melting and not decomposition, a view supported by the phase relations of $CaCO_3$ (Ivanov and Deutsch 2002). In addition, it appears that the impact melting of impure dolomites resulted in a dolomitic melt that crystallized calcite, leaving behind a residual Mg-rich melt that quenched to a glass. Detailed studies of impactites from other impact sites are needed in order to see if the results from Haughton are also applicable elsewhere. However, the recognition of carbonate melts at the Ries and Chicxulub structures, suggests that this may indeed be the case.

Acknowledgments–This study represents a component of the Ph.D. thesis of G.R.O. and was funded by the Natural Sciences and Engineering Research Council of Canada (NSERC) through research grants to J.G.S. Field studies were conducted under the auspices of the NASA Haughton-Mars Project with support provided to P.L. (P.I.) in part by the US National Aeronautics and Space Administration (NASA), the SETI Institute, and the Mars Institute. We are grateful to the Polar Continental Shelf Project (Natural Resources Canada), the Nunavut Research Institute, and the Communities of Grise Fiord and Resolute Bay for their support. We thank Alain Berinstain, Colleen Lenahan, Samson Ootoovak, Nesha Trenholm and everyone involved in the NASA Haughton-Mars Project for assistance during the HMP 1999–2003 field seasons. Douglas Hall provided valuable help during SEM studies. Cliff Shaw is thanked for very helpful discussions. Bevan French and Ann Therriault are thanked for their detailed and constructive reviews. PASSC publication number 40. This is contribution HMPSCI 2004-001.

Editorial Handling—Dr. Richard Grieve

REFERENCES

Barker D. S. 1989. Field relations of carbonatites. In *Carbonatites: Genesis and evolution*, edited by Bell K. London: Unwin Hyman. pp. 38–69.

Bell K., Kjarsgaard B. A., and Simonetti A. 1998. Carbonatites—Into the twenty-first century. *Journal of Petrology* 39:1839–1845.

Brooker R. A. 1998. The effect of CO_2 saturation on immiscibility between silicate and carbonate liquids: An experimental study. *Journal of Petrology* 39:1905–1915.

Brooker R. A., Kohn S. C., Holloway J. R., and McMillan P. F. 2001. Structural controls on the solubility of CO_2 in silicate melts—Part I: Bulk solubility data. *Chemical Geology* 174:225–239.

Bunch T. E., Grieve R. A. F., Lee P., McKay C. P., Rice J. W., Schutt J. W., and Zent A. 1998. Haughton Mars 97—II: Preliminary observations on highly shocked crystalline basement rocks on the Haughton Impact Crater (abstract #1307). 29th Lunar and Planetary Science Conference. CD-ROM.

Carstens H. 1975. Thermal history of impact melt rocks in the Fennoscandian Shield. *Contributions to Mineralogy and Petrology* 50:145–155.

Claeys P., Heuschkel S., Lounejeva-Baturina E., Sanchez R. G., and Stöffler D. 2003. The suevite of drill hole Yucatàn 6 in the Chicxulub impact crater. *Meteoritics & Planetary Science* 38: 1299–1317.

Dence M. R. 1971. Impact melts. *Journal of Geophysical Research* 76:5552–5565.

Dressler B. O. and Reimold W. U. 2001. Terrestrial impact melt rocks and glasses. *Earth Science Reviews* 56:205–284.

Dressler B. O., Sharpton V. L., Schwandt C. S., and Ames D. 2004. Impactites of the Yaxcopoil-1 drilling site, Chicxulub impact structure: Petrography, geochemistry, and depositional environment. *Meteoritics & Planetary Science* 39:857–878.

Fanelli M. F., Cava N., and Wyllie P. J. 1986. Calcite and dolomite without portlandite at a new eutectic in $CaO-MgO-CO_2-H_2O$, with applications to carbonatites. Proceedings, 13th General Meeting of the International Mineralogical Association. pp. 313–322.

Fisher R. V. and Schmincke H. U. 1984. *Pyroclastic rocks*. Berlin: Springer-Verlag. 472 p.

Frisch T. and Thorsteinsson R. 1978. Haughton astrobleme: A mid-Cenozoic impact crater, Devon Island, Canadian Arctic Archipelago. *Arctic* 31:108–124.

Graup G. 1999. Carbonate-silicate liquid immiscibility upon impact melting: Ries Crater, Germany. *Meteoritics & Planetary Science* 34:425–438.

Grieve R. A. F. 1975. Petrology and chemistry of impact melt at Mistastin Lake crater, Labrador. *Geological Society of America Bulletin* 86:1617–1629.

Grieve R. A. F. 1987. Terrestrial impact structures. *Annual Reviews of Earth and Planetary Science* 15:245–270.

Grieve R. A. F. 1988. The Haughton impact structure: Summary and synthesis of the results of the HISS Project. *Meteoritics* 23:249–254.

Grieve R. A. F. and Cintala M. J. 1992. An analysis of differential impact crater scaling and implications for the terrestrial record. *Meteoritics* 27:526–538.

Grieve R. A. F., Dence M. R., and Robertson P. B. 1977. Cratering processes: As interpreted from the occurrence of impact melts. In *Impact and explosion cratering*, edited by Roddy D. J., Pepin R. O., and Merrill R. B. New York: Pergamon Press. pp. 791–814.

Harmer R. E. and Gittins J. 1997. The case for primary, mantle-derived carbonatite magma. *Journal of Petrology* 39:1895–1903.

Hawke B. R. and Head J. W. 1977. Impact melt on lunar crater rims. In *Impact and explosion cratering*, edited by Roddy D. J., Pepin R. O., and Merrill R. B. New York: Pergamon Press. pp. 815–841.

Hörz F., Ostertag R., and Rainey D. A. 1983. Bunte Breccia of the Ries: Continuous deposits of large impact craters. *Reviews of Geophysics and Space Physics* 21:1667–1725.

Howard K. A. and Wilshire H. G. 1975. Flows of impact melt at lunar craters. *Journal of Research of the United States Geological Survey* 3:237–251.

Ivanov B. A. and Deutsch A. 2002. The phase diagram of $CaCO_3$ in relation to shock compression and decompression. *Physics of the Earth and Planetary Interiors* 129:131–143.

Jessburger E. K. 1988. ^{40}Ar-^{39}Ar dating of the Haughton impact structure. *Meteoritics* 23:233–234.

Jones A. P., Claeys P., and Heuschkel S. 2000. Impact melting of carbonates from the Chicxulub Crater. In *Impacts and the early Earth*, edited by Gilmour I. and Koeberl C. New York: Springer. pp. 343–361.

Kieffer S. W. 1971. Shock metamorphism of Coconino sandstone at Meteor Crater, Arizona. *Journal of Geophysical Research* 76: 5449–5473.

Kieffer S. W. and Simonds C. H. 1980. The role of volatiles and lithology in the impact cratering process. *Reviews of Geophysics and Space Physics* 18:143–181.

Kieffer S. W., Phakey D. P., and Christie J. M. 1976. Shock processes in porous quartzite: Transmission electron microscope observations and theory. *Contributions to Mineralogy and Petrology* 59:41–93.

Kring D. A., Hörz F., Zürcher L., and Urrutia Fucugauchi J. 2004. Impact lithologies and their emplacement in the Chicxulub impact crater: Initial results from the Chicxulub Scientific Drilling Project, Yaxcopoil, Mexico. *Meteoritics & Planetary Science* 39:879–897.

Lee W. J. and Wyllie P. J. 2000. The system CaO-MgO-SiO_2-CO_2 at 1 GPa, metasomatic wehrlites, and primary carbonatite magmas. *Contributions to Mineralogy and Petrology* 138:214–228.

Lee W. J., Fanelli M. F., Cava N., and Wyllie P. J. 2000. Calciocarbonatite and magnesiocarbonatite rocks and magmas represented in the system CaO-MgO-CO_2-H_2O at 0.2 GPa. *Mineralogy and Petrology* 48:225–256.

Lofgren G. 1970. Experimental devitrification rate of rhyolite glass. *Geological Society of America Bulletin* 81:553–560.

Marshall R. R. 1961. Devitrification of natural glass. *Geological Society of America Bulletin* 72:1493–1520.

Masaitis V. L. 1994. Impactites of the Popigai impact crater. In *Large meteorite impacts and planetary evolution*, edited by Dressler B. O., Grieve R. A. F., and Sharpton V. L. Special Paper #293. Boulder, Colorado: Geological Society of America. pp. 153–162.

McPhie J., Doyle M., and Allen R. 1993. *Volcanic textures: A guide to the interpretation of textures in volcanic rocks*. Hobart: Tasmanian Government Printing Office. 196 p.

Milton D. J., Glikson, A. Y., and Brett R. 1996. Gosses Bluff—A latest Jurassic impact structure, central Australia. Part 1: geological structure, stratigraphy, and origin. *Journal of Australian Geology and Geophysics* 16:453–486.

Melosh H. J. 1989. *Impact cratering: A geologic process*. New York: Oxford University Press. 245 p.

Metzler A., Ostertag R., Redeker H. J., and Stöffler D. 1988. Composition of the crystalline basement and shock metamorphism of crystalline and sedimentary target rocks at the Haughton impact crater. *Meteoritics* 23:197–207.

Morrison R. H. and Oberbeck V. R. 1978. A composition and thickness model for lunar impact crater and basin deposits. Proceedings, 9th Lunar and Planetary Science Conference. pp. 3763–3785.

Mysen B. O. 1976. The role of volatiles in silicate melts: Solubility of carbon dioxide and water in feldspar, pyroxene and felbspathoid melts to 30 kbar and 1625 °C. *American Journal of Science* 276:969–996.

Mysen B. O., Arculus R. J., and Eggler D. H. 1975. Solubility of carbon dioxide in melts of andesite, tholeiite and olivine nephelinite composition to 30 kbar pressure. *Contributions to Mineralogy and Petrology* 53:227–239.

Oberbeck V. R. 1975. The role of ballistic erosion and sedimentation in lunar stratigraphy. *Reviews in Geophysics and Space Physics* 13:337–362.

Osinski G. R. 2003. Impact glasses in fallout suevites from the Ries impact structure, Germany: An analytical SEM study. *Meteoritics & Planetary Science* 38:1641–1667.

Osinski G. R. and Lee P. 2005. Intra-crater sedimentary deposits at the Haughton impact structure, Devon Island, Canadian High Arctic. *Meteoritics & Planetary Science* 40. This issue.

Osinski G. R. and Spray J. G. 2001. Impact-generated carbonate melts: Evidence from the Haughton structure, Canada. *Earth and Planetary Science Letters* 194:17–29.

Osinski G. R. and Spray J. G. 2003. Evidence for the shock melting of sulfates from the Haughton impact structure, Arctic Canada. *Earth and Planetary Science Letters* 215:357–270.

Osinski G. R., Grieve R. A. F., and Spray J. G. 2004. The nature of the groundmass of surficial suevites from the Ries impact structure, Germany, and constraints on its origin. *Meteoritics & Planetary Science* 39:1655–1683.

Osinski G. R., Lee P., Spray J. G., Parnell J., Lim D., Bunch T. E., Cockell C. S., and Glass B. 2005. Geological overview and cratering model of the Haughton impact structure, Devon Island, Canadian High Arctic. *Meteoritics & Planetary Science* 40. This issue.

Otsuka R. 1986. Recent studies on the decomposition of the dolomite group by thermal analysis. *Thermochimica Acta* 100:69–80.

Otto J. W. and Wyllie P. J. 2000. Relationships between silicate melts and carbonate-precipitating melts in CaO-MgO-SiO_2-CO_2-H_2O at 2 kbar. *Mineralogy and Petrology* 48:343–365.

Pohl J., Stöffler D., Gall H., and Ernstson K. 1977. The Ries impact crater. In *Impact and explosion cratering*, edited by Roddy D. J., Pepin R. O., and Merrill R. B. New York: Pergamon Press. pp. 343–404.

Redeker H. J. and Stöffler D. 1988. The allochthonous polymict breccia layer of the Haughton impact crater, Devon Island, Canada. *Meteoritics* 23:185–196.

Robertson P. B. and Grieve R. A. F. 1978. The Haughton impact structure. *Meteoritics* 23:615–618.

Schmitt R. T., Wittmann A., and Stöffler D. 2004. Geochemistry of drill core samples from Yaxcopoil-1, Chicxulub impact crater, Mexico. *Meteoritics & Planetary Science* 39:979–1001.

Scott D. and Hajnal Z. 1988. Seismic signature of the Haughton structure. *Meteoritics* 23:239–247.

Sherlock S., Kelley S., Parnell J., Green P., Lee P., Osinski G. R., and Cockell C. S. 2005. Re-evaluating the age of the Haughton impact event. *Meteoritics & Planetary Science* 40. This issue.

Stöffler D. and Grieve R. A. F. 1994. Classification and nomenclature of impact metamorphic rocks: A proposal to the IUGS subcommission on the systematics of metamorphic rocks (abstract). 24th Lunar and Planetary Science Conference. pp. 1347–1348.

Stöffler D. and Grieve R. A. F. 1996. IUGS classification and nomenclature of impact metamorphic rocks: Towards a final proposal (abstract). International Symposium on the Role of Impact Processes in the Geological and Biological Evolution of Planet Earth.

Stöffler D., Artemieva N. A., Ivanov B. A., Hecht L., Kenkmann T., Schmitt R. T., Tagle R., and Wittmann A. 2004. Origin and emplacement of the impact formations at Chicxulub, Mexico, as revealed by the ICDP deep drilling at Yaxcopoil-1 and by numerical modeling. *Meteoritics & Planetary Science* 39:1035–1067.

Thorsteinsson R. and Mayr U. 1987. The sedimentary rocks of Devon Island, Canadian Arctic Archipelago. Geological Survey of Canada Memoir #411. Ottawa: Geological Survey of Canada. 182 p.

Treiman A. H. 1989. Carbonatite magma: Properties and processes. In *Carbonatites: Genesis and evolution*, edited by Bell K. London: Unwin Hyman. pp. 89–104.

Tuchscherer M. G., Reimold W. U., Koeberl C., Gibson R. L., and de Bruin D. 2004. First petrographic results on impactites from the Yaxcopoil-1 borehole, Chicxulub structure, Mexico. *Meteoritics & Planetary Science* 39:899–930.

Whitehead J., Grieve R. A. F., and Spray J. G. 2002. Mineralogy and petrology of melt rocks from the Popigai impact structure, Siberia. *Meteoritics & Planetary Science* 37:623–647.